Mutual reinforcement of lymphotoxin-driven myositis and impaired autophagy in murine muscle

Juliane Bremer,[1] Judith Nagel,[2] Jana Zschüntzsch,[3] Kamil K Zajt,[1] Tayfun Palaz,[1] Thomas Blank,[4] Aylin Ikis,[1] Laura A. Fischer,[3] Anna S. M. Sensmeyer,[3] Lara Wiechers,[3] Josef J. Reichelt,[3] Kai P. Hofmann,[5] Monika J. Wolf,[6,7] Corinna Leuchtenberger,[5] Priyanka Tripathi,[1] Claudia Einer,[8] Hans Zischka,[2,8] Ulrike Rothermel,[5] Anna-L. Eck,[5] Regina Reimann,[6] Veronika Kana,[6,9] Elisabeth Rushing,[6] Adriano Aguzzi,[6] Marco Prinz,[4,10] David Liebetanz,[3] Francesca Odoardi,[11] Chao-Chung Kuo,[12] Joachim Weis,[1] Florian Kraft,[13] Jens Schmidt[3,14,15,†] and Mathias Heikenwälder[5,16,†]

[†]**These authors contributed equally to this work.**

Abstract

Inclusion body myositis (IBM) is a progressive muscle disorder characterized by inflammation and degeneration with altered proteostasis. To better understand the interrelationship between these two features, we aimed at establishing a novel preclinical mouse model.

First, we used quantitative PCR to determine expression of pro-inflammatory chemo- and cytokines including lymphotoxin (LT)-signaling pathway components in human skeletal muscle tissue diagnosed with myositis. Based on these results we generated a mouse model that we analyzed at the histological, ultrastructural, transcriptional, biochemical, and behavioral level. Lastly, we subjected this model to anti-inflammatory treatments.

After confirming and extending previous data on activation of lymphotoxin (LT)-signaling in human myositis, we generated distinct transgenic mouse lines co-expressing LTα and -β in skeletal muscle fibers. Transgenic mice displayed chronic myositis accompanied by dysregulated proteostasis, including an altered autophagolysosomal pathway that initially shows signs of activation and later exhaustion and decreased flux. To enhance the latter, we genetically impaired

autophagy in skeletal muscle cells. Autophagy impairment alone induced a pro-inflammatory transcriptional state, but no obvious cellular inflammation. However, the combination of LT-driven myositis with autophagy impairment induced the full spectrum of characteristic molecular and pathological features of IBM in skeletal muscle, including protein inclusions with typical ultrastructural morphology and mild mitochondrial pathology. Our attempts to treat the pathology by subjecting these mice to corticosteroids or anti-Thy1.2 antibodies mirrored recent treatment failures in humans, i.e., none of these treatments resulted in significant clinical improvement of motor performance or the transcriptional profile of muscle pathology.

In summary, these data provide evidence that inflammation and autophagy disruption play a synergistic role in the development of IBM-like muscular pathology. Furthermore, once established, IBM-like pathology in these mice, as in human IBM patients cannot be reverted or prevented from progression by conventional means of immunosuppression. We expect that this novel mouse model will help to identify future treatment modalities for IBM.

Author affiliations:

1 Institute of Neuropathology, University Hospital RWTH Aachen, 52074 Aachen, Germany

2 Institute of Toxicology and Environmental Hygiene, Technical University of Munich, School of Medicine and Health, 80802 Munich, Germany

3 Department of Neurology, University Medical Center Göttingen, 37075 Göttingen, Germany

4 Institute of Neuropathology, Faculty of Medicine, University of Freiburg, 79106 Freiburg, Germany

5 Department of Chronic Inflammation and Cancer, DKFZ Heidelberg, 69120 Heidelberg, Germany

6 Institute of Neuropathology, University Hospital Zürich, 8091 Zürich, Switzerland

7 Current address: Roche Pharma Research and Early Development (pRED), Roche Innovation Center Munich, 82377 Penzberg, Germany

8 Institute of Molecular Toxicology and Pharmacology, Helmholtz Munich, 85764 Neuherberg, Germany

9 Department of Neurology, University Hospital Zürich, 8091 Zürich, Switzerland

10 Signalling Research Centres BIOSS and CIBSS, University of Freiburg, 79106 Freiburg, Germany

11 Institute for Neuroimmunology and Multiple Sclerosis Research, University Medical Center Göttingen, 37075 Göttingen, Germany

12 Genomics Facility, IZKF Aachen, RWTH Aachen University, 52074 Aachen, Germany

13 Center for Human Genetics and Genomic Medicine, University Hospital RWTH Aachen, 52074 Aachen, Germany

14 Department of Neurology and Pain Treatment, Immanuel Klinik Rüdersdorf, University Hospital of the Brandenburg Medical School Theodor Fontane, Rüdersdorf, Germany

15 Faculty of Health Sciences Brandenburg, Brandenburg Medical School Theodor Fontane, Rüdersdorf bei Berlin, Germany

16 The M3 Research Institute, Eberhard-Karls University, 72016 Tübingen, Germany

Correspondence to: Juliane Bremer

Institute of Neuropathology, University Hospital RWTH Aachen, Pauwelsstrasse 30, 52074 Aachen, Germany

E-mail: jbremer@ukaachen.de

Correspondence may also be addressed to: Mathias Heikenwälder

Department of Chronic Inflammation and Cancer, DKFZ Heidelberg, Im Neuenheimer Feld 242, 69120 Heidelberg, Germany

E-mail: m.heikenwaelder@dkfz-heidelberg.de

Running title: Lymphotoxin and autophagy in myositis

Keywords: lymphotoxin; lymphotoxin signaling; NF-κB signaling; autophagy; inclusion body myositis; myositis

Introduction

Inclusion body myositis (IBM) belongs to a heterogenous group of idiopathic inflammatory myopathies (IIM)[1] that affects between 25 and 46 per million people, mostly above the age of 45 years.[2,3] Clinically, patients with IBM usually present with progressive asymmetric weakness and atrophy often affecting the quadriceps femoris and/ or finger flexors.[4] Histopathologically, IBM is characterized by two main features, inflammation and degeneration.[5] Initial diagnostic criteria allowed the diagnosis of IBM solely based on these pathological features,[6] while more recent diagnostic criteria also take clinical features into account[3] and define the pathological feature "inflammation" as endomysial inflammatory infiltrates and upregulation of MHC class I (MHCI).[3] $CD8^+$ cytotoxic T cells usually predominate in these endomysial inflammatory infiltrates and some of these T cells invade non-necrotic myofibers.[6,7] The second diagnostic criterion, "degeneration", is defined as the light microscopic presence of rimmed vacuoles and/ or protein accumulation or 15-18 nm filaments on electron microscopy.[3] These rimmed vacuoles consist of autophagic vacuoles and ubiquitin-positive multiprotein inclusions, containing numerous proteins associated with neurodegenerative disorders, such as β-amyloid, phosphorylated tau and phosphorylated TDP-43, prion protein, as well as p62.[8-11] At the cellular level, different biochemical pathways that can ameliorate protein accumulations, including endoplasmic reticulum (ER) stress/ unfolded protein response (UPR), autophagolysosomal pathway and proteasomal degradation are severely dysregulated in IBM. Accumulation of misfolded proteins in the ER leads to ER stress, which in turn activates the UPR as a protective mechanism. Increased expression of factors characteristic of UPR (*ATF4, CHOP, GRP78*, spliced *XBP-1*) were observed in IBM but not in vacuolar myopathy due to *GNE* mutation.[12-14] Activities of lysosomal enzymes cathepsin D and B were decreased and autophagosome maturation, i.e., LC3-II was increased in human IBM muscle fibers, suggesting disturbed autophagosomal activity.[8] Even though expression of proteasome subunits was increased, one proteasome subunit was biochemically interacting with protein inclusions in IBM and proteasomal proteolytic activities were reduced, suggesting that also the proteasomal degradation system is dysfunctional in IBM.[15] Furthermore, mitochondrial alterations, including

COX-deficient fibers, accumulation of abnormal mitochondria, sometimes reflected in the presence of ragged red fibers, and mitochondrial DNA deletions are frequently found in IBM.[7,16,17]

The simultaneous occurrence of inflammation and degenerative pathological features in IBM has triggered considerable debate regarding which is the primary cause and driver of the disease. To solve this "chicken and egg" problem, i.e., whether inflammation drives myodegeneration or whether primary degeneration leads to inflammation,[7,18,19] it is essential to better understand the interaction between these two pathologies. During the last decades, efforts have been invested to resolve this conundrum. Considerable evidence supports that IBM is an autoimmune/ inflammatory disease: Genetic studies show strong genetic linkage to autoimmunity-associated HLA variants[20] and IBM is associated with other autoimmune diseases such as Sjogren's syndrome.[21] Previous studies have shown that muscle fiber-invading $CD8^+$ T cells had restricted T-cell receptor sequences, suggesting that they are clonally expanded,[22] but a muscle antigen has remained unknown. Autoantibodies have been detected in around 25% (anti-VCP) to up to 50% (anti-cytosolic 5'-nucleotidase 1A (NT5c1A)) of IBM patients, with 15% being positive for both antibodies. These antibodies are however not specific for IBM[23-25] and the clinical value of anti-VCP antibodies in particular remains to be determined.[26] Few studies have shown links between inflammatory mediators and signs of disturbed proteostasis. Notably, the exposure of human myotubes to IL-1 beta caused upregulation of β-amyloid precursor protein APP with subsequent intracellular aggregation of β-amyloid, suggesting that pro-inflammatory mediators can induce β-amyloid-associated muscle cell degeneration, thus supporting inflammation as the primary event.[27]

However, there are also compelling arguments in favor of a primarily degenerative pathogenesis. For example, protein inclusions, i.e. paired helical filaments in IBM strikingly resemble those in neurodegenerative diseases such as Alzheimer's disease.[10,11] APP can contribute to myopathy since its overexpression caused mitochondrial abnormalities and COX negativity in cultured human muscle fibers.[28] In addition, muscle cell-specific *APP* overexpression induced late-onset mild myopathic changes characterized by increased number of internally located myonuclei and mostly granulocytic, but not lymphocytic inflammation in mice.[29] When *Mck*-driven *App* overexpression was genetically combined with an Alzheimer's disease associated mutation in *Presenilin1,* mice displayed T cellular inflammation and increased β-amyloid deposits in muscle fibers, but vacuoles, muscle fiber degeneration or typical inclusions like in IBM were still not

described.[30] Nuclear loss and the cytoplasmic accumulation of transactivation response element DNA binding protein 43 (TDP-43) into inclusions observed in IBM muscle[9,10] resemble pathological features typical for amyotrophic lateral sclerosis (ALS) and frontotemporal dementia (FTD).[31] Furthermore, ER stress was shown to activate proinflammatory NF-κB signaling[32,33] and exposure of human myoblasts and C2C12 mouse skeletal muscle cells to β-amyloid peptides lead to increased IL-6 expression that may in turn stimulate $CD8^+$ T cells.[34] These findings show that disturbed protein homeostasis can induce inflammation in skeletal muscle. MHCI upregulation in IBM is usually regarded as evidence in favor of a primarily inflammatory disease, but skeletal muscle-specific overexpression of MHCI in mice induced myopathic chances with protein accumulations, vacuolation and ER stress/ UPR induction in the absence of lymphocytes[35] - inflammatory infiltrates in this model were of macrophage/myeloid lineage only without detectable T or B cells.[36] The first compelling argument for a primary degenerative pathogenesis, however, is that immunotherapies, which are successful in treating other inflammatory myopathies, lack efficacy in IBM. Moreover, T-cell depletion by alemtuzumab (anti-CD52 antibody) resulted in only transient clinical stabilization in selected IBM patients.[37] However, this effect was inconsistent and there was no significant difference in molecular parameters in the muscle of alemtuzumab-treated IBM patients.[38] The second main argument in favor of a primary degenerative pathology is that prominent inflammatory infiltrates in addition to vacuolar myopathy can be found in the context of certain gene mutations causing vacuolar myopathy, including some cases of multisystem proteinopathy. Examples are facioscapulohumeral muscular dystrophy (FSHD),[39] and cases with mutations in the *valosin-containing protein (VCP)* gene, a multifunctional ATPase regulating autophagy and other cellular processes[40-43], the *TDP43 gene*[44] and the *UDP-N-acetylglucosamine-2-epimerase/N-acetylmannosamine kinase (GNE)* gene that is required for sialic acid biosynthesis.[45] Thus, gene defects, including those involved in proteostasis, can rarely trigger vacuolar myopathy with inflammation, presenting as "hereditary myositis". However, this is not a consistent finding in genetic myopathies. Furthermore, this secondary inflammation differs markedly from myositis, T cells do not typically invade intact muscle fibers, and clonal expansion remains to be determined.

An animal model with the two cardinal IBM-like features, lymphocytic inflammation and characteristic inclusions is unavailable to date. Given the importance of the inflammatory pathology in disease pathogenesis, we aimed at generating a mouse model with chronic

lymphocytic inflammation to determine the consequence of inflammation on the proteostasis machinery and muscle fiber integrity *in vivo*. Besides the involvement of interferon signaling in human myositis,[46] there is evidence of induced lymphotoxin signaling and activation of its downstream mediator NF-κB[47,48] in IIM,[49] including IBM, in which normal-appearing myofibers express LTβ, possibly reflecting early myofiber damage.[50] ER stress, observed in IBM can induce NF-κB in cultured human muscle fibers.[32] Interestingly, the autophagy regulator and cargo adapter p62, which accumulates in IBM inclusions is known to crosstalk with NF-κB signaling.[51,52] Here we provide further evidence that lymphotoxins and their target genes are upregulated in human IIM. By expressing LTα and -β specifically in skeletal muscle fibers, we established a transgenic mouse line (HSA-LTα/β) with chronic myositis. Chronic myositis was accompanied by dysregulated proteostasis, including the autophagolysosomal pathway. The genetic combination of lymphotoxin-driven inflammation and autophagy impairment in mice lead to characteristic molecular and myopathological features resembling IBM, including lymphocytic inflammation and protein inclusions with typical ultrastructural morphology.

Materials and methods

Mouse housing and permits

Animal procedures were performed in accordance with EU and Swiss animal laws and approved by the government of Zurich, Bavaria, Baden-Württemberg and Niedersachsen, respectively (reference number 200/2007, 35-9185.81/G-113/17, 33.9-42502-04-18/2916). Human specimens were provided by the Armed forces institute of Pathology (AFIP), Washington D.C. after approval by the local ethics committee and then processed anonymously. ATG5<tm1(flox)> mice (here referred to as $Atg5^{flox/flox}$) were kindly provided by Dr. Noboru Mizushima (University of Tokyo, Japan). B6.Cg-Tg(ACTA1-cre)79Jme/J (here termed ACTA-Cre) and B6.FVB(129S4)-Tg(Ckmm-cre)5Khn/J (here termed Ckmm-Cre) were obtained from The Jackson Laboratory. Analyzed mice were of mixed gender.

Generation of tg(HSA:LTα_HSA:LTβ) mice

Lymphotoxins were amplified from plasmid DNA and cloned between human alpha-skeletal actin (HSA) promoter (-1905 to +239), kindly provided by Edna Hardeman[53] and SV40 poly A tail. Linearized HSA-LTα and HSA-LTβ were co-injected into pro-nuclei and embryos were transferred into pseudo-pregnant C57BL/6J at Biomodels Austria GmbH (Biat) by Prof. Dr. Thomas Rülicke. Animals were maintained on C57BL/6J background under SPF conditions, see also supplementary methods.

Genotyping

DNA was extracted from tail or ear biopsies. For primer sequences see supplementary methods.

Quantitative real time PCR (qPCR)

MRNA was extracted and reversely transcribed. QPCR was performed using Sybr Green. For experimental details see supplementary methods. Results were displayed by heat maps, created using the ComplexHeatmap package in Bioconductor/ RStudio Version 4.3.0.[54,55].

Histology, immunohistochemistry, muscle fiber size determination

For detailed protocols see supplementary methods. Muscle fiber size distribution was determined on H&E stained cross sections of the quadriceps femoris muscle, using ImageJ.

Electron microscopy

Samples were fixed in 3% glutaraldehyde in Sörensen buffer, incubated in 1% osmium, then further processed and embedded in epon resin as described in the supplementary methods.

Behavioral tests before and during drug treatments

Tests were performed as previously described,[56] see also the supplementary methods.

In situ RNA-hybridization

RNA in situ hybridization was performed using the RNAscope 2.0 brown FFPE Assay for murine and the BOND RNAscope Brown Detection kit (Advanced Cell Diagnostic/ Leica) for human tissue according to the manufacturer's protocol. See also supplementary methods.

Mitochondrial DNA sequencing

Mitochondrial DNA was amplified using established primers[57]. Long-range PCR products were purified. Libraries were prepared, pooled and sequenced on a MinION sequencer. The resulting BAM files were aligned to the GRCm38 reference genome using minimap2, and structural variations were identified with Sniffles2.[58] See supplementary methods for details.

RNAseq

RNA processing, library preparation and sequencing are described in the supplementary methods. Data were aligned to the GRCh38p14 genome and counted with STAR Aligner,[59] further analyzed and visualized with BioJupies.[60] Integrated pathway analysis and visualization was done with Pathview[61].

Analysis of published human RNAseq data

We downloaded datasets from the Gene Expression Omnibus (GEO) database: GSE151757,[62] GSE220915.[63] Differentially expressed genes (DEGs) were determined in R. Adjusted p-values were calculated using DESeq2.[64] For details see supplementary methods.

Drug treatments

Mice were subjected to continuous behavioral tests from 90 days of age. Treatment was initiated 30 days later (at 120 days), see also supplementary methods.

Statistical analysis

Statistical analysis was mostly performed using GraphPad Prism9.3.1 (GraphPad Software). See figure legends for applied tests. For categorial immunohistochemical data, we used Fisher's exact test (GraphPad online tool). Chi-square test was used to compare the fiber size distribution. All displayed graphs show mean and standard deviation.

Additional methods

For additional details on Forelimb grip strength, hanging wire test, muscle MRI, Enzyme-linked immunosorbent assays (ELISA) and Western blot see the Supplementary material.

Results

Lymphotoxin and target gene expression in human IIM

IIMs in humans are characterized by signs of inflammation and skeletal muscle fiber necrosis and regeneration as well as atrophy (Figure 1A). Endomysial infiltrates mainly consist of T cells in polymyositis (PM) and IBM and $CD4^+$ T cells and B cells in dermatomyositis (DM).[65] In PM and IBM, some T cells invade non-necrotic muscle fibers. Typically, MHCI is upregulated on the sarcolemma. In IBM, the light microscopic correlate of "degeneration" is the presence of abnormal autophagic vacuoles ("rimmed vacuoles"). Immunohistochemically, there is accumulation of the autophagy regulator and cargo adaptor p62[52] combined with the aggregation of proteins such as phospho-TDP43 (Figure 1A). To identify candidate pathomechanisms that could facilitate the establishment of suitable animal models, we examined the expression of several cyto- and chemokines in human inflammatory myopathies using qPCR. We found significant upregulation of several cyto- and chemokines, i.e. *LTα* was upregulated in PM, while LT/ NF-κB target genes[47,48,66-69] were upregulated in DM *(CCL19, CXCL10* and *BAFF)* and IBM *(CCL5* and *CCL19)*, respectively. The activation of NF-κB pathways was in line with previous investigations on human myositis[49,50,70] (Figure 1B-C). Using in situ hybridization and immunohistochemistry, we observed LTα and LTβ as well as LTβR expression in inflammatory infiltrates as well as in

muscle cells in IBM (Figure 1D-E). Previously published RNAseq data of human myositis did not specifically uncover enhanced LT signaling in IBM.[62,63] We integrated both published data sets, analyzed the expression of selected LT signaling-associated genes and observed a strong and significant upregulation of *LTα, LTβ* and LT target genes in IBM (Figure 1F). Other IIMs[63], such as immune-mediated necrotizing myopathy (IMNM), anti-synthetase syndrome (AS) and DM also showed upregulation of *LTα*. In AS and DM we also observed a significant, albeit weaker upregulation of *LTβ* (Supplementary figure 1). A previous study demonstrated a significant increase of *CXCL10* and *CCL5,* but not of *CXCL13* and *CCL19,* in IBM compared to other inflammatory myopathies, suggesting that lymphotoxin target genes *CXCL10* and *CCL5* are particularly upregulated in IBM[71]. These results confirm and extend previous data[47-50] demonstrating that LT signaling and its downstream targets are activated in human IIM.

Lymphotoxin expression in skeletal muscle causes chronic myositis in mice

Considering that LT signaling is prominent in human IIM and its role in inducing chronic inflammation in other tissues, including liver,[72] kidney,[73] pancreas,[73,74] and brain,[75] we generated a mouse model of chronic myositis by co-expressing LTα and LTβ in skeletal muscle. We cloned both LTα and LTβ separately behind the HSA promoter and coinjected both transgenic constructs into pronuclei derived from C57BL/6J mice (Figure 2A). We obtained four founder mice that contained both transgenes, HSA-LTα and HSA-LTβ and transmitted these together through the germline, suggesting concatemeric genomic insertion (Figure 2B). Line #8 did not breed sufficiently and could not be maintained. Lines #8, #22 and #44 displayed strong ectopic expression in other organs, including heart, brain, kidney and lung. Therefore, line #19 was selected for further study and is termed HSA-LTα/β hereafter. *In situ* mRNA hybridization and LTα ELISA showed strong and sustained LTα and LTβ expression in skeletal muscle (quadriceps femoris) of 3, 6 and 10 months old HSA-LTα/β transgenic mice (Figure 2C-D). Histology revealed numerous foci of endomysial, often perivascular inflammatory infiltrates composed of $CD4^+$ and $CD8^+$ T cells as well as frequent $B220^+$ B cells and $CD68^+$ macrophages. MHCI showed focal sarcolemmal upregulation. Especially in older mice (9 months), we observed endomysial fibrosis

and the proliferation of fat tissue (Figure 2E). Quantitative PCR (qPCR) and RNAseq analysis of quadriceps femoris muscle confirmed the strong and sustained upregulation of LTα/β. We also observed strong and significant upregulation of several proinflammatory cyto- und chemokines, including the LT target genes like *Ccl19* and *Cxcl10*, in line with our previous observations in human IIMs (Figure 2F, Supplementary data). LTα/β upregulation was restricted to the skeletal muscle compared to other organs in HSA-LTα/β line #19 (Figure 2G). No obvious difference in pathology was observed between different muscles (Figure 2H).

Quantification of muscle fiber size distribution revealed considerable widening of the muscle fiber caliber spectrum with increased atrophic and hypertrophic muscle fibers in HSA-LTα/β mice compared to controls at 3 and 6 months as well as significantly atrophic fibers at 10 months of age (Figure 3A), resembling observations in human IIM (Figure 1A). This was accompanied by a reduction in the overall body weight of both male and female mice (Figure 3B). The quadriceps femoris, gastrocnemius and triceps brachii muscles showed a significantly lower weight in HSA-LTα/β transgenic mice compared to controls (Figure 3C). Relative muscle weight loss was higher in the lower extremity (51 ± 12% for the quadriceps, 46 ± 10% for the gastrocnemius) compared to the upper extremity (36 ± 13% for the triceps brachii, at 10 months of age). Accordingly, motor functions, i.e. grip strength (Figure 3D) and performance in the hanging wire test (Figure 3E) were significantly impaired in HSA-LTα/β transgenic mice compared to wild-type. These data demonstrate that skeletal muscle specific expression of LTα and LTβ leads to chronic myositis in mice that shares histological, molecular and clinical features of human IIM.

Chronic myositis induces organelle stress, alters autophagy and mitochondrial gene expression

Skeletal muscles of HSA-LTα/β transgenic mice significantly upregulate genes associated with the ER stress/UPR (Figure 4A). Upon accumulation of unfolded proteins, BiP dissociates from the ER intraluminal domains of three ER transmembrane receptors: (1) type I transmembrane protein inositol requiring 1 (Ire1α), (2) eukaryotic initiation factor 2α (eIF2α) kinase PERK and (3) activating transcription factor 6 (Atf6) to activate pathways, which in turn reduce accumulated

unfolded proteins by increasing their folding, increasing their degradation and/or decrease the transcription and/or translation.[76]

While we did not detect an increase of spliced *Xbp1*, a surrogate marker of Ire1 activation, we found transcriptional evidence of activation of the other UPR pathways. In the second pathway, Perk activation leads to eIF2α, phosphorylation, which in turn reduces protein synthesis of most mRNAs except *Atf4* and *Chop* whose translation increases. Atf4 then induces expression of the transcription factors *Chop* and *Atf3*.[76] Chop, in turn, increases transcription of *Ero1l*.[77] We observed significant upregulation of *Ero1l* at 3 months, of *Atf3* at 3 and 6 months and of *Chop* at 10 months (Figure 4A). Atf3 and Atf4 both bind to the promotor region of *Gadd34*, which was significantly upregulated at 3 months of age. In the third pathway, Atf6 translocates to the Golgi, where it is cleaved and activated; cleaved Atf6 is then transported to the nucleus, where it activates transcription of target genes such as *Grp78/BiP*[76]. We observed upregulation of *Grp78* at 6 months, but downregulation at 10 months (Figure 4A), suggesting a transient induction of the Atf6 pathway (Supplementary figure 2).

The significant upregulation of several glutathione peroxidases: cytosolic *Gpx1*, plasma *Gpx3*, phospholipid hydroperoxide *Gpx4* and *Gpx8* (Figure 4B) suggested induction of oxidative stress in HSA-LTα/β mice. Gpx family members are antioxidants that detoxify hydroperoxides by reducing them to the corresponding alcohols by the means of glutathione (GSH). However, specific functions of individual Gpx have been shown. Gpx4 regulates inflammatory signaling: NF-κB activation by IL-1, reduced leukotriene and prostanoid biosynthesis, prevents COX-2 expression. Superoxide dismutase 3 (Sod3) is a known regulator of signaling pathways during inflammation and was found to be upregulated in HSA-LTα/β mice (Figure 4B). *Nrf2*, a transcription factor that regulates expression of antioxidant proteins that protect against oxidative damage,[78] was initially down- (6 months) and later upregulated (10 months; Figure 4B).

In addition we observed alterations in the expression of genes related to autophagolysosomal pathways (Figure 4A, 4C-4D). Autophagy related 5 (Atg5) is essential for the extension of the phagophoric membrane in the autophagic vesicle. It forms a complex with Atg12 and Atg16LL1, which is necessary for conjugation of LC3-I to phosphatidylethanolamine (PE) to form LC3-II. *Atg5* was significantly and strongly upregulated at 3 and 6 months in HSA-LTα/β mice. Likewise *Beclin 1 (Becn1)*, another important regulator of autophagy was significantly increased at 6

months. Interestingly, at 10 months, we observed downregulation of *Atg5* and lysosomal *Cathepsin b (Ctsb)*, indicative of a disturbed autophagolysosomal pathway in HSA-LTα/β mice. Similarly, analysis of published human IBM RNAseq data[62,63] revealed downregulation of autophagy-related genes *ATG5* and *BECN1, CTSB* was upregulated and *HSPB1* was downregulated in IBM (Figure 4D). While altered expression of *BECN1* and *CTSB* was also observed in other IIMs, the regulation of *ATG5* appears to be specific for IBM, and *HSPB1* was upregulated in other IIMs (Supplementary figure 1).[63]

The quantity of LC3-II protein has been suggested as a suitable indicator of autophagic activity.[79] We therefore measured LC3-II in skeletal muscle of HSA-LTα/β and wild-type mice by Western blot analysis (Figure 4E-F) at 6 and 10 months of age.

At 6 months, HSA-LTα/β muscle showed significantly reduced levels of total LC3 and LC3-I, while the LC3-II/LC3-I ratio remained unaltered. I.e. LC3-I was reduced along with LC3-II (Figure 4E-F), as reported after prolonged starvation.[79] Combined with the transcriptional upregulation of autophagy-related genes (*Atg5* and *Becn1*) described above, this suggests prolonged/ sustained autophagic activity in middle aged HSA-LTα/β. The LC3/LC3-I accumulation and decreased LC3-II/LC3-I ratio in HSA-LTα/β muscle at 10 months combined with the transcriptional downregulation of autophagy and lysosmal-related gene expression (*Atg5* and *Ctsb*) suggest an impaired autophagic flux (Figure 4E-F, Supplementary figure 2-3), most likely reflecting exhaustion due to overload. These changes were similar, but less pronounced compared to "controls" with skeletal muscle specific autophagy disruption by depleting *Atg5* - by combining the *creatine kinase, M-type (Ckmm)* promoter driven Cre expressing transgene (Ckmm-Cre) with the floxed *Atg5* allele ($Atg5^{fl/fl}$), later termed HSA-LT;CreAtg5 (see below).

In line with disturbed proteostasis and autophagolysosomal pathway, we detected occasional accumulation of ubiquitinated proteins in some muscle fibers of HSA-LTα/β mice compared to controls and altered distribution of $LAMP2^{+}$ lysosomes (Figure 4F), similar to observations in humans.[80]

To better understand the cellular and molecular pathophysiological mechanisms that lead to the observed shifts with ageing, we performed RNAseq of wild-type and HSA-LTα/β muscles, both at 6 and 9 months. Beside the strong upregulation of proinflammatory genes in HSA-LTα/β,

including *Tbx21*, an established marker of highly differentiated T cells specific for IBM,[71] along with *Il2*, another marker of Tc1 cytotoxic T-cells, but not of DM signature genes.[71] Gene set enrichment analysis (GSEA) revealed profound upregulation of mitochondria-associated genes with ageing in wild-type muscle, which was not observed in HSA-LTα/β mice. Instead, HSA-LTα/β mice showed significantly reduced mitochondria-associated gene expression compared to wild-type (Supplementary data). Furthermore, in line with previous observations,[81] UPR-related gene expression was dysregulated in ageing wild-type muscle. Hence, age-related changes in proteostasis- and mitochondria-associated gene expression might contribute to the apparent shifts in transcriptional alterations in HSA-LTα/β muscle. Immunoproteasome subunits *Psmb8-10*, but not subunits 1-7, were upregulated in HSA-LTα/β muscle (Supplementary data), similar to the specific upregulation of *PSMB9-10*, previously detected in human IBM compared to other inflammatory myopathies.[71] GSEA further revealed downregulation of ubiquitination- and mTOR signaling-associated genes in HSA- LTα/β muscle, pointing at possible mechanisms that could alter the autophagolysosomal pathway activity.

Based on the failure of HSA-LTα/β muscle to upregulate mitochondria associated genes with ageing, the transcriptional signs of oxidative stress in HSA-LTα/β mice and in light of the prominent mitochondrial pathology in human IIM, especially in IBM, we examined the ultrastructure of mitochondria in these mice. We found considerable mitochondrial swelling, but no definitive signs of major chronic mitochondrial pathology such as paracrystalline inclusions, major structural abnormalities of cristae including concentric forms or abnormal mitophagy (Figure 4G) at this point.

Together, these results suggest that chronic myositis in HSA-LTα/β mice is associated with unspecific alterations of proteostasis and autophagy. However, there is no major, potentially self-perpetuating and self-reinforcing autophagy disturbances or other major degenerative pathologies such as abnormal protein inclusions.

Genetically impairing autophagy in LT-induced myositis adds IBM-like inclusions to the phenotype

We hypothesized that in LT-driven chronic myositis, temporary induction of the autophagic flux prevents the formation of IBM-like protein inclusions. In older HSA-LTα/β mice and in human IBM muscle biopsy tissue, *Atg5/ATG5* was downregulated in line with impaired autophagy reported in human IBM.[82,83] Therefore, we aimed at speeding up and enhancing its downregulation and at the same time determining the role of autophagy in chronic inflammation by specifically depleting *Atg5* in the skeletal muscle of HSA-LTα/β transgenic mice. To do so, we combined the Ckmm-Cre transgene with the floxed *Atg5* allele (*Atg5*$^{fl/fl}$; Figure 5A). Double genetically modified mice (*HSA-LTα/β*$^{+}$ *Ckmm-Cre*$^{+}$ *Atg5*$^{fl/fl}$), hereafter termed HSA-LT;CreAtg5 mice displayed muscular atrophy compared to mice lacking *Atg5* only (*Ckmm-Cre*$^{+}$ *Atg5*$^{fl/fl}$), hereafter termed CreAtg5. Muscle volumes were determined by muscle MRI (Figure 5B-C). HSA-LT;CreAtg5 mice showed histological signs of inflammation similar to HSA-LTα/β mice, including endomysial inflammatory infiltrates and MHCI upregulation (Figure 5D-F), while CreAtg5 mice did not show inflammation. HSA-LT;CreAtg5 mice were weaker, i.e. had reduced grip strength and shorter hanging time, compared to CreAtg5 controls (Figure 5G-H). In addition, HSA-LT;CreAtg5 mice showed disrupted distribution of LAMP2^{+} lysosomes, and displayed numerous ubiquitin- and p62-positive and occasional phospho-TDP43 positive inclusions (Figure 6A). Electron microscopy of HSA-LT;CreAtg5 mouse muscles revealed partial disintegration of sarcomeres and abundant accumulation of granular and fibrillar material often resembling tubulofilamentous inclusions characteristic of human IBM. Mitochondria were focally increased and often showed transitions in abnormal osmiophilic, myelin-like autophagic material, indicative of abnormal mitophagy (Figure 6B). Although we did not detect mitochondrial DNA deletions in "bulk" long-read sequencing, combined COX-SDH enzyme histochemistry of the quadriceps muscle revealed mitochondrial abnormalities in HSA-LTα/β and especially in HSA-LT;CreAtg5 mice that were not observed in wild-type animals. COX-positive mitochondria showed a slightly more irregular distribution in HSA-LTα/β compared to wild-type (Figure 6D). The distribution of COX-positive mitochondria was even more irregular in HSA-LT;CreAtg5 and single muscle fibers showed mosaicisms, i.e. focal subpopulation of COX-negative mitochondria next to COX-positive mitochondria in the same fiber. Irregularities were found in all and COX mosaicism was found in

6 of 8 HSA-LT;CreAtg5 mice. This mosaicism was absent in the HSA-LTα/β and wild-type mice tested (Figure 6D). Hence mitochondrial pathology is present, but minimal in our model.

The upregulation of chemo- and cytokines at 6 month of age in HSA-LT;CreAtg5 mice was similar to that observed in HSA-LTα/β mice (Figure 7A). In line with our expectation, we observed transcriptional signs of disturbed proteostasis in skeletal muscle with *Atg5* depletion alone (CreAtg5; Figure 6B), including increased expression of UPR-associated genes like *Grp78* and *Chop* (Figure 7B). Notably, we observed cyto- and chemokine upregulation, including LT/ NF-κB target genes *Ccl5*[84] and *Cxcl10* (IP-10[67,68]) in CreAtg5 (Figure 7A). This demonstrates that chronic inflammation not only leads to autophagy dysregulation, but also vice versa, autophagy impairment leads to proinflammatory signaling, i.e. activation of the LT/ NF-κB signal transduction pathway and only caused sarcolemmal MHCI upregulation in some cases. This proinflammatory transcriptional milieu in CreAtg5 mice was, however, not sufficient to induce histological signs of inflammation such as endomysial lymphocytic infiltrates (Figure 5D-E). Besides, we confirmed the upregulation of autophagy-related genes *Atg5, Atg12, Becn1*, observed *Ctsb* upregulation and oxidative stress-related upregulation of *Gpx1* and *Sod3* as well as downregulation of *Ncf2* in HSA-LTα/β mice at 6 months in this independent experiment (Figure 7 –in line with previous results in Figure 4A-B). *Tumorous imaginal disc 1 (Tid1)*, also called *DnaJ homolog subfamily A member 3 (DnaJA3)* was the only gene specifically downregulated in HSA-LT;CreAtg5 mice (Figure 7B). Tid1 is a multifunctional protein that acts as a co-chaperone of mtHsp70. Of note, Tid1 is a regulator of autophagy[85] and several signaling pathways including Wnt and Trk. Interestingly, it also represses activity of NF-κB through interaction with IkB[86]. In fact, Tid1 was shown to control various biological processes. These included muscle energy homeostasis, development, myogenesis[87] and synapse formation by binding to muscle specific kinase (MuSK),[88] mitochondrial fragmentation,[89] β-amyloid production by controlling BACE1 levels and mediating β-amyloid induced ROS generation and neuronal cell death in Alzheimer's diseases[90] – a disease associated with cellular protein inclusions similar to IBM. We also observed upregulation of *Amyloid precursor protein (App)* and *alpha-b-Crystallin (Cryab)*, previously observed in human myositis, especially in IBM.[91,92]

Muscle-specific RING finger protein-1 (MuRF1) is an E3 ubiquitin ligase in cardiac and skeletal muscles that is upregulated during skeletal muscle atrophy and mediates ubiquitin proteasome

system-mediated degradation of sarcomeric muscle proteins[93-95] and may contribute to muscle fiber atrophy observed in HSA-LTα/β mice. Furthermore, *Tweak* was upregulated in CreAtg5, HSA-LTα/β and HSA-LT;CreAtg5 mice as previously described in human IBM muscle where TWEAK is supposed to reduce activation and differentiation of muscle precursor cells and may induce muscle atrophy.[96]

IBM-like myositis in mice is resistant to anti-inflammatory treatments

In humans, anti-inflammatory treatments, including steroids, intravenous immunoglobulins (IVIG), anti-CD52 (alemtuzumab) have shown efficacy in PM and DM. Unfortunately, none of these approaches have shown any long-lasting therapeutic effects in IBM.[37,38,97-99] We tested the efficacy of these therapies, including prednisolone, and lymphocyte-depleting anti-Thy1.2 in our mouse model. To determine motor function in these mice, behavioral performance was continuously monitored in untreated and treated mice, starting at 90 days of age - before and during treatment from 120 to 160 days of age (Figure 8A). None of these treatments improved motor performance in mice with chronic myositis (Figure 8, Supplementary figures 4-5). To verify the effect of these treatments on inflammatory cells, we determined T cell densities in the liver of these mice and found a significant reduction after treatment (Figure 8B-C). To detect milder effects on the skeletal muscle upon treatment, we analyzed transcriptional profiles. We observed minor alterations following prednisolone (Figure 8E) but no significant effects on gene expression in anti-Thy1.2 treated mice (Supplementary figure 6). This shows that, once initiated, chronic myositis is resistant to anti-inflammatory treatment in HSA-LTα/β and HSA-LT;CreAtg5 mice.

Discussion

LT-driven inflammation with inclusions in mice resembles several but not all features of human IBM

Our mouse model of chronic inflammatory and vacuolar myopathy recapitulates some of the key features seen in human IBM, including lymphocytic endomysial inflammation and chronic

necrotizing and vacuolar myopathy with prominent alterations of proteostasis and autophagy associated with tubulofilamentous inclusions and abnormal autophagic vacuoles. However, inflammatory myopathy in HSA-LT;CreAtg5 mice also showed features that differ from typical human IBM cases. First, B cells outnumbered T cells in the lymphocytic infiltrates in mouse muscle, in contrast to mostly T cells, especially $CD8^+$ cytotoxic T cells in human IBM.[6,7] Still, B-cell-rich inflammation has been described in rare cases of human IBM,[100] and terminally differentiated B cells – plasma cells – as well as immunoglobulin gene transcripts are well established adjacent to scattered B cells in IBM as well as in PM,[101,102] suggesting that they contribute to pathogenesis. Furthermore, the applied B cell marker B220 also labels plasma cell-precursors, the plasmablasts.[103] In our model, B cells likely infiltrate the muscle because lymphotoxin induces *CXCL13* expression (Figure 7A) that in turn is known to attract B cells.[104] Of note, *CXCL13* is also upregulated in human IBM (Figure 1E) and a recent paper using single nucleus RNAseq combined with spatial transcriptomics revealed a B cell-rich inflammatory niche in human IBM.[82]

Mitochondrial abnormalities are frequently observed in IBM in humans.[7,16,17] These findings include COX-negative fibers, mitochondrial DNA deletions, paracrystalline inclusions and structural abnormalities of cristae such as their concentric arrangement, as well as signs of dysfunctional mitophagy.[105,106] Whereas abnormal mitophagy associated with transcriptional signs of mitochondrial oxidative stress are prominent features in HSA-LTα/β and HSA-LT;CreAtg5 mice, anomalies of cristae architecture are minimal (Figure 4B,4G,6B). Paracrystalline inclusions have not been observed. However, we are not aware of paracrystalline inclusions and other major structural mitochondrial changes consistently being described in mouse models of mitochondrial myopathies. For example, *Polg* mutant mice ultrastructurally display dissolution of mitochondrial cristae and swelling in cardiac muscle at the ultrastructural level[107]. These findings are similar to the widened spaces between mitochondrial cristae observed by us in HSA-LTα/β mouse skeletal muscle fibers (Figure 4G). Of note, paracrystalline inclusions are a feature of human patients with *POLG* mutations,[108] but were not reported in *Polg* mutant mice. Hence, mice might be protected from mitochondrial paracrystalline inclusion formation, possibly due to a higher volume of mitochondria in murine compared to human skeletal muscle.[109] Despite the lack of paracrystalline inclusions, and mitochondrial DNA deletions in bulk sequencing, mitochondria are involved in chronic inflammatory and vacuolar myopathy in our mice. This is demonstrated by the failure of

the inflamed muscle in our mouse model to upregulate mitochondria-associated gene expression with ageing based on the RNAseq data (Supplementary data) and by the irregular distribution of COX-positive mitochondria in transgenic mice and especially by the single mosaic fibers with COX-negative mitochondria in otherwise COX-positive fibers in HSA-LT;CreAtg5 mice (Figure 6D).

In this context, it is interesting to note that PM with mitochondrial pathology (PM-Mito[110]), more recently referred to as inflammatory myopathy with mitochondrial pathology in muscle (IM-Mito), may be considered a precursor or early form of IBM with little or no pTDP-43 aggregation,[111] implying that mitochondrial alterations could be an early event in the pathophysiological cascade leading to the full blown picture of IBM.[111,112] Alterations in autophagic degradation pathways have been found in both, IBM and PM with mitochondrial alterations, suggesting a link between mitochondrial and autophagy dysregulation in myositis in humans.[111] On a molecular level, there are possible links between ER stress, oxidative stress and autophagy impairment in HSA-LTα/β mice. UPR-induced *Ero1l* observed in HSA-LTα/β mice is a H_2O_2 producing enzyme that has been shown to increase oxidative stress upon ER stress.[113] In mesenchymal stem cells (MSCs), depletion of autophagic proteins such as LC3B, Becn1 increased susceptibility of cells to oxidative stress.[114] However, how ER stress pathways and mitochondria intersect in myositis pathogenesis remains to be determined.[115]

Interdependence of inflammation and impaired proteostasis

Our expression data describe an upregulation of lymphotoxin and lymphotoxin β receptor target genes in human inflammatory myopathies, confirming and extending previous observations.[49,50,70] Targeted expression of lymphotoxins in muscle fibers of our transgenic HSA-LTα/β mice induced chronic inflammatory myopathy that shares characteristic clinical and pathological features with human myositis, including necrotizing myopathy with muscular atrophy and weakness, lymphomonocytic endomysial infiltrates upregulation of chemo-and cytokine transcription and of sarcolemmal MHCI and endomysial fibrosis. Lymphotoxin-driven chronic lymphomonocytic myositis in these mice alters autophagolysosomal pathways, induces ER stress and leads to focal accumulation of ubiquitin-positive inclusions as well as oxidative stress and mild mitochondrial

alterations, in line with observations in human IBM[116]. This suggests that activation of the NF-κB pathway and inflammation perturb proteostasis and induce a mild, unspecific degenerative pathology. Chronic myositis did not suffice to induce the full spectrum of IBM pathology. We hypothesized that activation of the autophagolysosomal flux partially compensates and impedes further dysregulation of proteostasis and protein aggregation in chronic myositis in middle aged HSA-LTα/β mice (6 months). To speed up and enhance autophagy impairment, which we only observe later in older HSA-LTα/β mice (10 months), we genetically impaired autophagy in mice with lymphotoxin-driven myositis and then observed the full spectrum of IBM-associated pathology – a myopathic phenotype with inflammation and IBM-like degeneration (Figure 5-6). If the additional autophagy impairment is actually a requirement, i.e. the straw that breaks the camel's back or if this occurs when chronic myositis persists longer still remains unknown. Autophagy impairment alone did not induce myositis. Although there was significant upregulation of some chemo- and cytokines, suggesting a pro-inflammatory molecular milieu, and signs of ER stress, we did not observe endomysial lymphomonocytic cell infiltrates or MHCI upregulation. This suggests that autophagy impairment and ER stress can at most contribute to inflammation but not independently induce the complete picture of myositis. Nevertheless, our data underscore that inflammation and autophagy impairment act synergistically and jointly contribute to potentially self-perpetuating and self-reinforcing disturbances, eventually resulting in IBM-like abnormal protein inclusions and disturbed mitophagy.

Molecular links between inflammation and degenerative features

Several previous observations indicate that inflammation and degenerative features in IBM are intertwined. MHCI, which is upregulated on the sarcolemma of muscle fibers, was shown to induce ER stress, which in turn leads to a release of chemo- and cytokines from C2C12 myoblasts[117]. ER stress is well known to activate the ER overload response (EOR) that involves the upregulation of NF-κB pathway and modulation of the inflammatory response. In fact, ER stress/EOR are not exclusive to IBM, but also observed in PM and DM.[70] Different pathways regulating proteostasis are linked, including ER stress and autophagy. In cultured human muscle fibers, ER stress induction leads to increased levels of LC3-II and increased maturation of autophagosomes, but decreased activities of lysosomal cathepsins D and B.[8]

Our results support these observations and point to previously unrecognized crosstalk pathways. In mice with impaired autophagy in skeletal muscle, we observed upregulated ER stress-related genes and chemo- and cytokines including NF-κB target genes, probably through the EOR. Activation of the NF-κB pathway in the muscles of HSA-LTα/β mice in turn induced ER stress. We further observed strong upregulation of Tribbles homolog 3 (Trib3), a regulator of ER stress-induced apoptosis and NF-κB signaling[118] in CreAtg5 mice, possibly linking ER stress with NF-κB signaling and inflammation.

In addition, we found dysregulated expression of further genes that may be involved in these interactions. We observed significant upregulation of superoxide dismutase *Sod3* in HSA-LTα/β and HSA-LT;CreAtg5 mice (Figure 4&7). All Sods possess anti-oxidative properties. Within this family, Sod3 is secreted into the extracellular matrix, where it ameliorates oxidative stress- and inflammation-induced tissue damage. The anti-inflammatory function of Sod3 is in part exerted by downregulating NF-κB signaling.[119] Inflammatory cytokines and influenza A virus infection have been shown to enhance Sod3 expression.[120,121] Overexpression of Sod3 in turn was found to enhance autophagy.[122] Sod3 may therefore link and regulate inflammation, oxidative stress and autophagy in our mouse model and exert potentially a protective function.

Subunits *Psmb9-10* of the immunoproteasome that breaks down intracellular proteins for antigen presentation by MHCII,[123] were upregulated in HSA-LTα/β mice similar to human IBM.[71] This potentially links inflammation, proteostasis regulation and mitochondrial dysfunction as *PSMB9* is induced to regulate cellular proteostasis upon mitochondrial dysfunction.[124]

Although we noted at least a temporary upregulation of several genes involved in UPR and oxidative stress, including *Grp78, Chop, Atf3, Ero1l* and *Gpx* genes (Figure 4&7), we observed early and strong downregulation of *Hsp27/Hspb1* in HSA-LTα/β mice (Figure 4). Hsp27 has been shown to act as a chaperone and antioxidative protein and ameliorates fibrotic processes in kidney disease.[125] Its downregulation may perturb proteostasis and induce endomysial fibrosis in HSA-LTα/β mice. Similarly, downregulation of *XBP1* promotes fibrosis in injured kidneys[126] where overwhelming ER stress results in selective *Xbp1u* and *Xbp1s* downregulation,[127] possibly contributing to endomysial fibrosis in HSA-LTα/β mice.

Failure of anti-inflammatory treatments and self-perpetuation of chronic inflammatory and vacuolar myopathy

The resistance to therapeutic T-cell depletion by prednisolone and anti-Thy1.2 observed in our murine model is in line with the lack of a consistent, at the most, subtle clinical improvement following anti-inflammatory treatments[97] as well as the absence of significant differences in molecular parameters in alemtuzumab/ anti-CD52 antibody-treated IBM patients.[38] Recently, the further characterization of T cells in human IBM muscle revealed an increased number of highly differentiated $CD8^+$ cytotoxic T cells expressing killer cell lectin-like receptor G1 (KLRG1).[71] These $CD8^+$ $KLRG1^+$ T cells may be refractory to immunotherapy and may explain the resistance of IBM patients to anti-inflammatory therapies.[71,128] However, the persistent loss of TDP-43 function and rimmed vacuoles after T-cell depletion in mice with xenografts of human IBM tissue suggested that T-cell depletion cannot alter muscle degenerative pathology in IBM,[129] even when $CD8^+$ $KLRG1^+$ T cells are removed. This suggests that inflammation is either secondary or required to initiate pathology, however, not essential for disease progression and self-perpetuation. The selective, antibody-mediated depletion of $KLRG^+$ T cells in an ongoing human clinical trial in IBM will provide further insight (ClinicalTrials.gov ID NCT05721573).

An alternative explanation for treatment failure in chronic inflammatory and vacuolar myopathy in our mouse model and human IBM is impaired muscle regeneration after degeneration. In neuromuscular diseases, satellite cells, the muscle stem cells proliferate and differentiate for repair and regeneration.[130] Satellite cells may be impaired or exhausted in neuromuscular diseases. Pax7 is expressed in satellite cells and is required for their regenerative function in adult skeletal muscle.[131] The significant reduction of Pax7 in CreAtg5, and even more in HSA-LTα/β and HSA-LT;CreAtg5 mice suggests fewer satellite cell number and therefore decreased regenerative potential. Our finding may appear to contrast the increase of $Pax7^+$ satellite cells previously described in human PM/DM and IBM.[132,133] However, they are in line with evidence of reduced satellite cell plasticity shown in long-term IBM-patients[134]. In addition, the resistance of IBM patients to the myostatin blocker bimagrumab, which increases the volume of normal muscle,[135] argues for a defective regenerative response in IBM.

The lack of response to treatment could also be due to hitherto unknown factors that we also do not know in human patients with IBM.

In the future, our mouse model of chronic inflammatory and vacuolar myopathy will be used to test novel therapeutic strategies including combinatorial strategies of anti-inflammatory treatment and molecules targeting protein homeostasis.

Data availability

The authors confirm that the data supporting the findings of this study are available within the article and its Supplementary material.

Acknowledgements

We would like to thank Iris Iben, Florian Müller, Danijela Heide, Jenny Hetzer, Jay Tracy, Regina Nitsche, Janine Rick, Sebastian Gießelmann, and Klimentina Popzhelyazkova, for technical assistance. The method for calf muscle volume quantification was provided and installed by Dr. Peter Allegrini Novartis Pharma AG. Software was developed by Jeff Tsao and Michael Hensen (Novartis Pharma AG).

Funding

M.H. was supported by The Helmholtz Future topic Inflammation and Immunology, Zukunftssthema "Immunology and Inflammation" (ZT-0027) (M.H.); The Rainer Hoenig Stiftung (M.H.); The Research Foundation Flanders (FWO) under grant 30826052 (EOS Convention MODEL-IDI) (M.H.); Seed funding from HI-TRON (M.H.).

Competing interests

M.J.W. is employed by Roche Diagnostics GmbH, the author declares no conflict of interest that pertain to this work. The other authors declare no competing interests.

Supplementary material

Supplementary material is available at *Brain* online.

References

1. Tanboon J, Uruha A, Stenzel W, Nishino I. Where are we moving in the classification of idiopathic inflammatory myopathies? *Curr Opin Neurol*. Oct 2020;33(5):590-603. doi:10.1097/WCO.0000000000000855

2. Callan A, Capkun G, Vasanthaprasad V, Freitas R, Needham M. A Systematic Review and Meta-Analysis of Prevalence Studies of Sporadic Inclusion Body Myositis. *J Neuromuscul Dis*. 2017;4(2):127-137. doi:10.3233/JND-160198

3. Rose MR, Group EIW. 188th ENMC International Workshop: Inclusion Body Myositis, 2-4 December 2011, Naarden, The Netherlands. *Neuromuscul Disord*. Dec 2013;23(12):1044-55. doi:10.1016/j.nmd.2013.08.007

4. Dimachkie MM, Barohn RJ. Inclusion body myositis. *Neurol Clin*. Aug 2014;32(3):629-46, vii. doi:10.1016/j.ncl.2014.04.001

5. Yunis EJ, Samaha FJ. Inclusion body myositis. *Lab Invest.* Sep 1971;25(3):240-8.

6. Griggs RC, Askanas V, DiMauro S, et al. Inclusion body myositis and myopathies. *Ann Neurol*. Nov 1995;38(5):705-13. doi:10.1002/ana.410380504

7. Greenberg SA. Inclusion body myositis: clinical features and pathogenesis. *Nat Rev Rheumatol*. May 2019;15(5):257-272. doi:10.1038/s41584-019-0186-x

8. Nogalska A, D'Agostino C, Terracciano C, Engel WK, Askanas V. Impaired autophagy in sporadic inclusion-body myositis and in endoplasmic reticulum stress-provoked cultured human muscle fibers. *Am J Pathol*. Sep 2010;177(3):1377-87. doi:10.2353/ajpath.2010.100050

9. Hiniker A, Daniels BH, Lee HS, Margeta M. Comparative utility of LC3, p62 and TDP-43 immunohistochemistry in differentiation of inclusion body myositis from polymyositis and related inflammatory myopathies. *Acta Neuropathol Commun*. Jul 1 2013;1:29. doi:10.1186/2051-5960-1-29

10. Dubourg O, Wanschitz J, Maisonobe T, et al. Diagnostic value of markers of muscle degeneration in sporadic inclusion body myositis. *Acta Myol*. Oct 2011;30(2):103-8.

11. Askanas V, Engel WK, Bilak M, Alvarez RB, Selkoe DJ. Twisted tubulofilaments of inclusion body myositis muscle resemble paired helical filaments of Alzheimer brain and contain hyperphosphorylated tau. *Am J Pathol*. Jan 1994;144(1):177-87.

12. Vattemi G, Engel WK, McFerrin J, Askanas V. Endoplasmic reticulum stress and unfolded protein response in inclusion body myositis muscle. *Am J Pathol*. Jan 2004;164(1):1-7. doi:10.1016/S0002-9440(10)63089-1

13. Corona-Sanchez EG, Martinez-Garcia EA, Lujano-Benitez AV, et al. Autoantibodies in the pathogenesis of idiopathic inflammatory myopathies: Does the endoplasmic reticulum stress response have a role? *Front Immunol*. 2022;13:940122. doi:10.3389/fimmu.2022.940122

14. Nogalska A, D'Agostino C, Engel WK, et al. Activation of the Unfolded Protein Response in Sporadic Inclusion-Body Myositis but Not in Hereditary GNE Inclusion-Body Myopathy. *J Neuropathol Exp Neurol*. Jun 2015;74(6):538-46. doi:10.1097/NEN.0000000000000196

15. Fratta P, Engel WK, McFerrin J, Davies KJ, Lin SW, Askanas V. Proteasome inhibition and aggresome formation in sporadic inclusion-body myositis and in amyloid-beta precursor protein-overexpressing cultured human muscle fibers. *Am J Pathol*. Aug 2005;167(2):517-26. doi:10.1016/s0002-9440(10)62994-x

16. Lindgren U, Roos S, Hedberg Oldfors C, Moslemi AR, Lindberg C, Oldfors A. Mitochondrial pathology in inclusion body myositis. *Neuromuscul Disord*. Apr 2015;25(4):281-8. doi:10.1016/j.nmd.2014.12.010

17. Oldfors A, Moslemi AR, Jonasson L, Ohlsson M, Kollberg G, Lindberg C. Mitochondrial abnormalities in inclusion-body myositis. *Neurology*. Jan 24 2006;66(2 Suppl 1):S49-55. doi:10.1212/01.wnl.0000192127.63013.8d

18. Benveniste O, Stenzel W, Hilton-Jones D, Sandri M, Boyer O, van Engelen BG. Amyloid deposits and inflammatory infiltrates in sporadic inclusion body myositis: the inflammatory egg comes before the degenerative chicken. *Acta Neuropathol*. May 2015;129(5):611-24. doi:10.1007/s00401-015-1384-5

19. Weihl CC, Mammen AL. Sporadic inclusion body myositis - a myodegenerative disease or an inflammatory myopathy. *Neuropathol Appl Neurobiol*. Feb 2017;43(1):82-91. doi:10.1111/nan.12384

20. Rothwell S, Cooper RG, Lundberg IE, et al. Immune-Array Analysis in Sporadic Inclusion Body Myositis Reveals HLA-DRB1 Amino Acid Heterogeneity Across the Myositis Spectrum. *Arthritis Rheumatol*. May 2017;69(5):1090-1099. doi:10.1002/art.40045

21. Migkos MP, Sarmas I, Somarakis GA, Voulgari PV, Tsamis KI, Drosos AA. Sjogren Syndrome Associated with Inflammatory Muscle Diseases. *Mediterr J Rheumatol*. Jun 2018;29(2):92-96. doi:10.31138/mjr.29.2.92

22. Bender A, Behrens L, Engel AG, Hohlfeld R. T-cell heterogeneity in muscle lesions of inclusion body myositis. *J Neuroimmunol*. Apr 1 1998;84(1):86-91. doi:10.1016/s0165-5728(97)00246-4

23. Pluk H, van Hoeve BJ, van Dooren SH, et al. Autoantibodies to cytosolic 5'-nucleotidase 1A in inclusion body myositis. *Ann Neurol*. Mar 2013;73(3):397-407. doi:10.1002/ana.23822

24. Amlani A, Choi MY, Tarnopolsky M, et al. Anti-NT5c1A Autoantibodies as Biomarkers in Inclusion Body Myositis. *Front Immunol*. 2019;10:745. doi:10.3389/fimmu.2019.00745

25. Larman HB, Salajegheh M, Nazareno R, et al. Cytosolic 5'-nucleotidase 1A autoimmunity in sporadic inclusion body myositis. *Ann Neurol*. Mar 2013;73(3):408-18. doi:10.1002/ana.23840

26. Amlani A, Choi MY, Buhler KA, et al. Anti-Valosin-Containing Protein (VCP/p97) Autoantibodies in Inclusion Body Myositis and Other Inflammatory Myopathies. *ACR Open Rheumatol*. Jan 2023;5(1):10-14. doi:10.1002/acr2.11510

27. Schmidt J, Barthel K, Wrede A, Salajegheh M, Bahr M, Dalakas MC. Interrelation of inflammation and APP in sIBM: IL-1 beta induces accumulation of beta-amyloid in skeletal muscle. *Brain*. May 2008;131(Pt 5):1228-40. doi:10.1093/brain/awn053

28. Askanas V, McFerrin J, Baque S, Alvarez RB, Sarkozi E, Engel WK. Transfer of beta-amyloid precursor protein gene using adenovirus vector causes mitochondrial abnormalities in cultured normal human muscle. *Proc Natl Acad Sci U S A*. Feb 6 1996;93(3):1314-9. doi:10.1073/pnas.93.3.1314

29. Sugarman MC, Yamasaki TR, Oddo S, et al. Inclusion body myositis-like phenotype induced by transgenic overexpression of beta APP in skeletal muscle. *Proc Natl Acad Sci U S A*. Apr 30 2002;99(9):6334-9. doi:10.1073/pnas.082545599

30. Kitazawa M, Green KN, Caccamo A, LaFerla FM. Genetically augmenting Abeta42 levels in skeletal muscle exacerbates inclusion body myositis-like pathology and motor deficits in transgenic mice. *Am J Pathol*. Jun 2006;168(6):1986-97. doi:10.2353/ajpath.2006.051232

31. Neumann M, Sampathu DM, Kwong LK, et al. Ubiquitinated TDP-43 in frontotemporal lobar degeneration and amyotrophic lateral sclerosis. *Science*. Oct 6 2006;314(5796):130-3. doi:10.1126/science.1134108

32. Nogalska A, Wojcik S, Engel WK, McFerrin J, Askanas V. Endoplasmic reticulum stress induces myostatin precursor protein and NF-kappaB in cultured human muscle fibers: relevance to inclusion body myositis. *Exp Neurol*. Apr 2007;204(2):610-8. doi:10.1016/j.expneurol.2006.12.014

33. Pahl HL, Baeuerle PA. The ER-overload response: activation of NF-kappa B. *Trends Biochem Sci*. Feb 1997;22(2):63-7. doi:10.1016/s0968-0004(96)10073-6

34. Baron P, Galimberti D, Meda L, et al. Production of IL-6 by human myoblasts stimulated with Abeta: relevance in the pathogenesis of IBM. *Neurology*. Nov 13 2001;57(9):1561-5. doi:10.1212/wnl.57.9.1561

35. Freret M, Drouot L, Obry A, et al. Overexpression of MHC class I in muscle of lymphocyte-deficient mice causes a severe myopathy with induction of the unfolded protein response. *Am J Pathol*. Sep 2013;183(3):893-904. doi:10.1016/j.ajpath.2013.06.003

36. Li CK, Knopp P, Moncrieffe H, et al. Overexpression of MHC class I heavy chain protein in young skeletal muscle leads to severe myositis: implications for juvenile myositis. *Am J Pathol*. Sep 2009;175(3):1030-40. doi:10.2353/ajpath.2009.090196

37. Dalakas MC, Rakocevic G, Schmidt J, et al. Effect of Alemtuzumab (CAMPATH 1-H) in patients with inclusion-body myositis. *Brain*. Jun 2009;132(Pt 6):1536-44. doi:10.1093/brain/awp104

38. Schmidt K, Kleinschnitz K, Rakocevic G, Dalakas MC, Schmidt J. Molecular treatment effects of alemtuzumab in skeletal muscles of patients with IBM. *BMC Neurol*. Apr 16 2016;16:48. doi:10.1186/s12883-016-0568-5

39. Reilich P, Schramm N, Schoser B, et al. Facioscapulohumeral muscular dystrophy presenting with unusual phenotypes and atypical morphological features of vacuolar myopathy. *J Neurol*. Jul 2010;257(7):1108-18. doi:10.1007/s00415-010-5471-1

40. Watts GD, Thomasova D, Ramdeen SK, et al. Novel VCP mutations in inclusion body myopathy associated with Paget disease of bone and frontotemporal dementia. *Clin Genet*. Nov 2007;72(5):420-6. doi:10.1111/j.1399-0004.2007.00887.x

41. Ferrari V, Cristofani R, Tedesco B, et al. Valosin Containing Protein (VCP): A Multistep Regulator of Autophagy. *Int J Mol Sci*. Feb 9 2022;23(4)doi:10.3390/ijms23041939

42. Iannibelli E, Gibertini S, Cheli M, et al. VCP-related myopathy: a case series and a review of literature. *Acta Myol*. 2023;42(1):2-13. doi:10.36185/2532-1900-244

43. Shinjo SK, Oba-Shinjo SM, Lerario AM, Marie SKN. A Brazilian family with inclusion body myopathy associated with Paget's disease of bone and frontotemporal dementia linked to the VCP pGly97Glu mutation. *Clin Rheumatol*. Apr 2018;37(4):1129-1136. doi:10.1007/s10067-017-3913-1

44. Ervilha Pereira P, Schuermans N, Meylemans A, et al. C-terminal frameshift variant of TDP-43 with pronounced aggregation-propensity causes rimmed vacuole myopathy but not ALS/FTD. *Acta Neuropathol*. Jun 2023;145(6):793-814. doi:10.1007/s00401-023-02565-1

45. Krause S, Schlotter-Weigel B, Walter MC, et al. A novel homozygous missense mutation in the GNE gene of a patient with quadriceps-sparing hereditary inclusion body myopathy associated with muscle inflammation. *Neuromuscul Disord*. Dec 2003;13(10):830-4. doi:10.1016/s0960-8966(03)00140-8

46. Gasparotto M, Franco C, Zanatta E, et al. The interferon in idiopathic inflammatory myopathies: Different signatures and new therapeutic perspectives. A literature review. *Autoimmun Rev*. Jun 2023;22(6):103334. doi:10.1016/j.autrev.2023.103334

47. Gommerman JL, Browning JL. Lymphotoxin/light, lymphoid microenvironments and autoimmune disease. *Nat Rev Immunol*. Aug 2003;3(8):642-55. doi:10.1038/nri1151

48. Sun SC. Non-canonical NF-kappaB signaling pathway. *Cell Res*. Jan 2011;21(1):71-85. doi:10.1038/cr.2010.177

49. Monici MC, Aguennouz M, Mazzeo A, Messina C, Vita G. Activation of nuclear factor-kappaB in inflammatory myopathies and Duchenne muscular dystrophy. *Neurology*. Mar 25 2003;60(6):993-7. doi:10.1212/01.wnl.0000049913.27181.51

50. Creus KK, De Paepe B, Weis J, De Bleecker JL. The multifaceted character of lymphotoxin beta in inflammatory myopathies and muscular dystrophies. *Neuromuscul Disord*. Aug 2012;22(8):712-9. doi:10.1016/j.nmd.2012.04.012

51. Su J, Liu F, Xia M, et al. p62 participates in the inhibition of NF-kappaB signaling and apoptosis induced by sulfasalazine in human glioma U251 cells. *Oncol Rep*. Jul 2015;34(1):235-43. doi:10.3892/or.2015.3944

52. Komatsu M, Kageyama S, Ichimura Y. p62/SQSTM1/A170: physiology and pathology. *Pharmacol Res*. Dec 2012;66(6):457-62. doi:10.1016/j.phrs.2012.07.004

53. Brennan KJ, Hardeman EC. Quantitative analysis of the human alpha-skeletal actin gene in transgenic mice. *J Biol Chem*. Jan 5 1993;268(1):719-25.

54. Gu Z, Eils R, Schlesner M. Complex heatmaps reveal patterns and correlations in multidimensional genomic data. *Bioinformatics*. Sep 15 2016;32(18):2847-9. doi:10.1093/bioinformatics/btw313

55. Gu Z. Complex heatmap visualization. *iMeta*. 2022;1(3):e43. doi:10.1002/imt2.43

56. Zschuntzsch J, Jouvenal PV, Zhang Y, et al. Long-term human IgG treatment improves heart and muscle function in a mouse model of Duchenne muscular dystrophy. *J Cachexia Sarcopenia Muscle*. Aug 2020;11(4):1018-1031. doi:10.1002/jcsm.12569

57. Emser SV, Schaschl H, Millesi E, Steinborn R. Extension of Mitogenome Enrichment Based on Single Long-Range PCR: mtDNAs and Putative Mitochondrial-Derived Peptides of Five Rodent Hibernators. *Front Genet*. 2021;12:685806. doi:10.3389/fgene.2021.685806

58. Smolka M, Paulin LF, Grochowski CM, et al. Detection of mosaic and population-level structural variants with Sniffles2. *Nat Biotechnol*. Oct 2024;42(10):1571-1580. doi:10.1038/s41587-023-02024-y

59. Dobin A, Davis CA, Schlesinger F, et al. STAR: ultrafast universal RNA-seq aligner. *Bioinformatics*. Jan 1 2013;29(1):15-21. doi:10.1093/bioinformatics/bts635

60. Torre D, Lachmann A, Ma'ayan A. BioJupies: Automated Generation of Interactive Notebooks for RNA-Seq Data Analysis in the Cloud. *Cell Syst*. Nov 28 2018;7(5):556-561 e3. doi:10.1016/j.cels.2018.10.007

61. Luo W, Pant G, Bhavnasi YK, Blanchard SG, Jr., Brouwer C. Pathview Web: user friendly pathway visualization and data integration. *Nucleic Acids Res*. Jul 3 2017;45(W1):W501-W508. doi:10.1093/nar/gkx372

62. Johari M, Vihola A, Palmio J, et al. Comprehensive transcriptomic analysis shows disturbed calcium homeostasis and deregulation of T lymphocyte apoptosis in inclusion body myositis. *J Neurol*. Aug 2022;269(8):4161-4173. doi:10.1007/s00415-022-11029-7

63. Casal-Dominguez M, Pinal-Fernandez I, Pak K, et al. Coordinated local RNA overexpression of complement induced by interferon gamma in myositis. *Sci Rep*. Feb 4 2023;13(1):2038. doi:10.1038/s41598-023-28838-z

64. Love MI, Huber W, Anders S. Moderated estimation of fold change and dispersion for RNA-seq data with DESeq2. *Genome Biol*. 2014;15(12):550. doi:10.1186/s13059-014-0550-8

65. Franco C, Gatto M, Iaccarino L, Ghirardello A, Doria A. Lymphocyte immunophenotyping in inflammatory myositis: a review. *Curr Opin Rheumatol*. Nov 1 2021;33(6):522-528. doi:10.1097/BOR.0000000000000831

66. Wang ZZ, Song J, Wang H, et al. B Cell-Activating Factor Promotes B Cell Survival in Ectopic Lymphoid Tissues in Nasal Polyps. *Front Immunol*. 2020;11:625630. doi:10.3389/fimmu.2020.625630

67. Krinninger P, Brunner C, Ruiz PA, et al. Role of the adipocyte-specific NF-kappaB activity in the regulation of IP-10 and T cell migration. *Am J Physiol Endocrinol Metab*. Feb 2011;300(2):E304-11. doi:10.1152/ajpendo.00143.2010

68. Zhou Y, Wang S, Ma JW, et al. Hepatitis B virus protein X-induced expression of the CXC chemokine IP-10 is mediated through activation of NF-kappaB and increases migration of leukocytes. *J Biol Chem*. Apr 16 2010;285(16):12159-68. doi:10.1074/jbc.M109.067629

69. Mebius RE. Organogenesis of lymphoid tissues. *Nat Rev Immunol*. Apr 2003;3(4):292-303. doi:10.1038/nri1054

70. Nagaraju K, Casciola-Rosen L, Lundberg I, et al. Activation of the endoplasmic reticulum stress response in autoimmune myositis: potential role in muscle fiber damage and dysfunction. *Arthritis Rheum*. Jun 2005;52(6):1824-35. doi:10.1002/art.21103

71. Greenberg SA, Pinkus JL, Kong SW, Baecher-Allan C, Amato AA, Dorfman DM. Highly differentiated cytotoxic T cells in inclusion body myositis. *Brain*. Sep 1 2019;142(9):2590-2604. doi:10.1093/brain/awz207

72. Haybaeck J, Zeller N, Wolf MJ, et al. A lymphotoxin-driven pathway to hepatocellular carcinoma. *Cancer Cell*. Oct 6 2009;16(4):295-308. doi:10.1016/j.ccr.2009.08.021

73. Kratz A, Campos-Neto A, Hanson MS, Ruddle NH. Chronic inflammation caused by lymphotoxin is lymphoid neogenesis. *J Exp Med*. Apr 1 1996;183(4):1461-72. doi:10.1084/jem.183.4.1461

74. Seleznik GM, Reding T, Romrig F, et al. Lymphotoxin beta receptor signaling promotes development of autoimmune pancreatitis. *Gastroenterology*. Nov 2012;143(5):1361-1374. doi:10.1053/j.gastro.2012.07.112

75. O'Connor T, Zhou X, Kosla J, et al. Age-Related Gliosis Promotes Central Nervous System Lymphoma through CCL19-Mediated Tumor Cell Retention. *Cancer Cell*. Sep 16 2019;36(3):250-267 e9. doi:10.1016/j.ccell.2019.08.001

76. Read A, Schroder M. The Unfolded Protein Response: An Overview. *Biology (Basel)*. Apr 29 2021;10(5)doi:10.3390/biology10050384

77. Marciniak SJ, Yun CY, Oyadomari S, et al. CHOP induces death by promoting protein synthesis and oxidation in the stressed endoplasmic reticulum. *Genes Dev*. Dec 15 2004;18(24):3066-77. doi:10.1101/gad.1250704

78. Scannevin RH, Chollate S, Jung MY, et al. Fumarates promote cytoprotection of central nervous system cells against oxidative stress via the nuclear factor (erythroid-derived 2)-like 2 pathway. *J Pharmacol Exp Ther*. Apr 2012;341(1):274-84. doi:10.1124/jpet.111.190132

79. Mizushima N, Yoshimori T. How to interpret LC3 immunoblotting. *Autophagy*. Nov-Dec 2007;3(6):542-5. doi:10.4161/auto.4600

80. Tsuruta Y, Furuta A, Furuta K, Yamada T, Kira J, Iwaki T. Expression of the lysosome-associated membrane proteins in myopathies with rimmed vacuoles. *Acta Neuropathol*. Jun 2001;101(6):579-84. doi:10.1007/s004010000329

81. Takasugi M, Nonaka Y, Takemura K, et al. An atlas of the aging mouse proteome reveals the features of age-related post-transcriptional dysregulation. *Nat Commun*. Oct 2 2024;15(1):8520. doi:10.1038/s41467-024-52845-x

82. Wischnewski S, Thawel T, Ikenaga C, et al. Cell type mapping of inflammatory muscle diseases highlights selective myofiber vulnerability in inclusion body myositis. *Nat Aging*. Jul 2024;4(7):969-983. doi:10.1038/s43587-024-00645-9

83. Canto-Santos J, Valls-Roca L, Tobias E, et al. Unravelling inclusion body myositis using a patient-derived fibroblast model. *J Cachexia Sarcopenia Muscle*. Apr 2023;14(2):964-977. doi:10.1002/jcsm.13178

84. Yeh DY, Wu CC, Chin YP, Lu CJ, Wang YH, Chen MC. Mechanisms of human lymphotoxin beta receptor activation on upregulation of CCL5/RANTES production. *Int Immunopharmacol*. Sep 2015;28(1):220-9. doi:10.1016/j.intimp.2015.06.010

85. Niu G, Zhang H, Liu D, et al. Tid1, the Mammalian Homologue of Drosophila Tumor Suppressor Tid56, Mediates Macroautophagy by Interacting with Beclin1-containing Autophagy Protein Complex. *J Biol Chem*. Jul 17 2015;290(29):18102-18110. doi:10.1074/jbc.M115.665950

86. Banerjee S, Chaturvedi R, Singh A, Kushwaha HR. Putting human Tid-1 in context: an insight into its role in the cell and in different disease states. *Cell Commun Signal*. Jul 19 2022;20(1):109. doi:10.1186/s12964-022-00912-5

87. Cheng LH, Hung KF, Lee TC, et al. Mitochondrial co-chaperone protein Tid1 is required for energy homeostasis during skeletal myogenesis. *Stem Cell Res Ther*. Dec 7 2016;7(1):185. doi:10.1186/s13287-016-0443-8

88. Linnoila J, Wang Y, Yao Y, Wang ZZ. A mammalian homolog of Drosophila tumorous imaginal discs, Tid1, mediates agrin signaling at the neuromuscular junction. *Neuron*. Nov 26 2008;60(4):625-41. doi:10.1016/j.neuron.2008.09.025

89. Elwi AN, Lee B, Meijndert HC, Braun JE, Kim SW. Mitochondrial chaperone DnaJA3 induces Drp1-dependent mitochondrial fragmentation. *Int J Biochem Cell Biol*. Aug 2012;44(8):1366-76. doi:10.1016/j.biocel.2012.05.004

90. Zhou C, Taslima F, Abdelhamid M, et al. Beta-Amyloid Increases the Expression Levels of Tid1 Responsible for Neuronal Cell Death and Amyloid Beta Production. *Mol Neurobiol*. Feb 2020;57(2):1099-1114. doi:10.1007/s12035-019-01807-2

91. Greenberg SA, Sanoudou D, Haslett JN, et al. Molecular profiles of inflammatory myopathies. *Neurology*. Oct 22 2002;59(8):1170-82. doi:10.1212/wnl.59.8.1170

92. Li K, Pu C, Huang X, Liu J, Mao Y, Lu X. Proteomic study of sporadic inclusion body myositis. *Proteome Sci*. 2014;12(1):45. doi:10.1186/s12953-014-0045-2

93. Bodine SC, Latres E, Baumhueter S, et al. Identification of ubiquitin ligases required for skeletal muscle atrophy. *Science*. Nov 23 2001;294(5547):1704-8. doi:10.1126/science.1065874

94. Clarke BA, Drujan D, Willis MS, et al. The E3 Ligase MuRF1 degrades myosin heavy chain protein in dexamethasone-treated skeletal muscle. *Cell Metab*. Nov 2007;6(5):376-85. doi:10.1016/j.cmet.2007.09.009

95. Cohen S, Brault JJ, Gygi SP, et al. During muscle atrophy, thick, but not thin, filament components are degraded by MuRF1-dependent ubiquitylation. *J Cell Biol*. Jun 15 2009;185(6):1083-95. doi:10.1083/jcb.200901052

96. Morosetti R, Gliubizzi C, Sancricca C, et al. TWEAK in inclusion-body myositis muscle: possible pathogenic role of a cytokine inhibiting myogenesis. *Am J Pathol*. Apr 2012;180(4):1603-13. doi:10.1016/j.ajpath.2011.12.027

97. Dalakas MC. Immunotherapy of myositis: issues, concerns and future prospects. *Nat Rev Rheumatol*. Mar 2010;6(3):129-37. doi:10.1038/nrrheum.2010.2

98. Gandiga PC, Ghetie D, Anderson E, Aggrawal R. Intravenous Immunoglobulin in Idiopathic Inflammatory Myopathies: a Practical Guide for Clinical Use. *Curr Rheumatol Rep*. Aug 2023;25(8):152-168. doi:10.1007/s11926-023-01105-w

99. Ruck T, Bittner S, Kuhlmann T, Wiendl H, Meuth SG. Long-term efficacy of alemtuzumab in polymyositis. *Rheumatology (Oxford)*. Mar 2015;54(3):560-2. doi:10.1093/rheumatology/keu484

100. Konomatsu K, Izumi R, Suzuki N, et al. A rare case of sporadic inclusion body myositis and rheumatoid arthritis exhibiting ectopic lymphoid follicle-like structures: a case report and literature review. *Neuromuscul Disord*. Sep 2021;31(9):870-876. doi:10.1016/j.nmd.2021.07.002

101. Greenberg SA, Bradshaw EM, Pinkus JL, et al. Plasma cells in muscle in inclusion body myositis and polymyositis. *Neurology*. Dec 13 2005;65(11):1782-7. doi:10.1212/01.wnl.0000187124.92826.20

102. Jiang R, Roy B, Wu Q, et al. The Plasma Cell Infiltrate Populating the Muscle Tissue of Patients with Inclusion Body Myositis Features Distinct B Cell Receptor Repertoire Properties. *Immunohorizons*. May 1 2023;7(5):310-322. doi:10.4049/immunohorizons.2200078

103. Pracht K, Meinzinger J, Daum P, et al. A new staining protocol for detection of murine antibody-secreting plasma cell subsets by flow cytometry. *Eur J Immunol*. Aug 2017;47(8):1389-1392. doi:10.1002/eji.201747019

104. Harrer C, Otto F, Radlberger RF, et al. The CXCL13/CXCR5 Immune Axis in Health and Disease-Implications for Intrathecal B Cell Activities in Neuroinflammation. *Cells*. Aug 25 2022;11(17)doi:10.3390/cells11172649

105. Askanas V, Engel WK, Nogalska A. Sporadic inclusion-body myositis: A degenerative muscle disease associated with aging, impaired muscle protein homeostasis and abnormal mitophagy. *Biochim Biophys Acta*. Apr 2015;1852(4):633-43. doi:10.1016/j.bbadis.2014.09.005

106. De Paepe B. Sporadic Inclusion Body Myositis: An Acquired Mitochondrial Disease with Extras. *Biomolecules*. Jan 7 2019;9(1)doi:10.3390/biom9010015

107. Lewis W, Day BJ, Kohler JJ, et al. Decreased mtDNA, oxidative stress, cardiomyopathy, and death from transgenic cardiac targeted human mutant polymerase gamma. *Lab Invest*. Apr 2007;87(4):326-35. doi:10.1038/labinvest.3700523

108. Van Goethem G, Dermaut B, Lofgren A, Martin JJ, Van Broeckhoven C. Mutation of POLG is associated with progressive external ophthalmoplegia characterized by mtDNA deletions. *Nat Genet*. Jul 2001;28(3):211-2. doi:10.1038/90034

109. Vincent AE, White K, Davey T, et al. Quantitative 3D Mapping of the Human Skeletal Muscle Mitochondrial Network. *Cell Rep*. Apr 2 2019;27(1):321. doi:10.1016/j.celrep.2019.03.051

110. Blume G, Pestronk A, Frank B, Johns DR. Polymyositis with cytochrome oxidase negative muscle fibres. Early quadriceps weakness and poor response to immunosuppressive therapy. *Brain*. Jan 1997;120 (Pt 1):39-45. doi:10.1093/brain/120.1.39

111. Temiz P, Weihl CC, Pestronk A. Inflammatory myopathies with mitochondrial pathology and protein aggregates. *J Neurol Sci*. Mar 15 2009;278(1-2):25-9. doi:10.1016/j.jns.2008.11.010

112. Kleefeld F, Uruha A, Schanzer A, et al. Morphologic and Molecular Patterns of Polymyositis With Mitochondrial Pathology and Inclusion Body Myositis. *Neurology*. Nov 15 2022;99(20):e2212-e2222. doi:10.1212/WNL.0000000000201103

113. Haynes CM, Titus EA, Cooper AA. Degradation of misfolded proteins prevents ER-derived oxidative stress and cell death. *Mol Cell*. Sep 10 2004;15(5):767-76. doi:10.1016/j.molcel.2004.08.025

114. Ghanta S, Tsoyi K, Liu X, et al. Mesenchymal Stromal Cells Deficient in Autophagy Proteins Are Susceptible to Oxidative Injury and Mitochondrial Dysfunction. *Am J Respir Cell Mol Biol*. Mar 2017;56(3):300-309. doi:10.1165/rcmb.2016-0061OC

115. Rayavarapu S, Coley W, Nagaraju K. Endoplasmic reticulum stress in skeletal muscle homeostasis and disease. *Curr Rheumatol Rep*. Jun 2012;14(3):238-43. doi:10.1007/s11926-012-0247-5

116. Askanas V, Engel WK. Sporadic inclusion-body myositis: conformational multifactorial ageing-related degenerative muscle disease associated with proteasomal and lysosomal inhibition, endoplasmic reticulum stress, and accumulation of amyloid-beta42 oligomers and phosphorylated tau. *Presse Med*. Apr 2011;40(4 Pt 2):e219-35. doi:10.1016/j.lpm.2010.11.024

117. Thoma A, Earl KE, Goljanek-Whysall K, Lightfoot AP. Major histocompatibility complex I-induced endoplasmic reticulum stress mediates the secretion of pro-inflammatory muscle-derived cytokines. *J Cell Mol Med*. Dec 2022;26(24):6032-6041. doi:10.1111/jcmm.17621

118. Fang N, Zhang W, Xu S, et al. TRIB3 alters endoplasmic reticulum stress-induced beta-cell apoptosis via the NF-kappaB pathway. *Metabolism*. Jun 2014;63(6):822-30. doi:10.1016/j.metabol.2014.03.003

119. Sah SK, Agrahari G, Kim TY. Insights into superoxide dismutase 3 in regulating biological and functional properties of mesenchymal stem cells. *Cell Biosci*. 2020;10:22. doi:10.1186/s13578-020-00386-3

120. Kemp K, Gray E, Mallam E, Scolding N, Wilkins A. Inflammatory cytokine induced regulation of superoxide dismutase 3 expression by human mesenchymal stem cells. *Stem Cell Rev Rep*. Dec 2010;6(4):548-59. doi:10.1007/s12015-010-9178-6

121. Chen F, Chen L, Liang J, et al. Potential Role of Superoxide Dismutase 3 (SOD3) in Resistance to Influenza A Virus Infection. *Antioxidants (Basel)*. Feb 2 2023;12(2)doi:10.3390/antiox12020354

122. Agrahari G, Sah SK, Kim TY. Superoxide dismutase 3 protects mesenchymal stem cells through enhanced autophagy and regulation of FoxO3a trafficking. *BMB Rep*. Jul 2018;51(7):344-349. doi:10.5483/bmbrep.2018.51.7.078

123. Zeng L, Chen K, Xiao F, et al. Potential common molecular mechanisms between Sjogren syndrome and inclusion body myositis: a bioinformatic analysis and in vivo validation. *Front Immunol*. 2023;14:1161476. doi:10.3389/fimmu.2023.1161476

124. Kim M, Serwa RA, Samluk L, et al. Immunoproteasome-specific subunit PSMB9 induction is required to regulate cellular proteostasis upon mitochondrial dysfunction. *Nat Commun*. Jul 11 2023;14(1):4092. doi:10.1038/s41467-023-39642-8

125. Vidyasagar A, Wilson NA, Djamali A. Heat shock protein 27 (HSP27): biomarker of disease and therapeutic target. *Fibrogenesis Tissue Repair*. May 7 2012;5(1):7. doi:10.1186/1755-1536-5-7

126. Chen JH, Wu CH, Jheng JR, et al. The down-regulation of XBP1, an unfolded protein response effector, promotes acute kidney injury to chronic kidney disease transition. *J Biomed Sci*. Jun 28 2022;29(1):46. doi:10.1186/s12929-022-00828-9

127. Chiang CK, Hsu SP, Wu CT, et al. Endoplasmic reticulum stress implicated in the development of renal fibrosis. *Mol Med*. 2011;17(11-12):1295-305. doi:10.2119/molmed.2011.00131

128. Greenberg SA. Pathogenesis of inclusion body myositis. *Curr Opin Rheumatol*. Nov 2020;32(6):542-547. doi:10.1097/BOR.0000000000000752

129. Britson KA, Ling JP, Braunstein KE, et al. Loss of TDP-43 function and rimmed vacuoles persist after T cell depletion in a xenograft model of sporadic inclusion body myositis. *Sci Transl Med*. Jan 19 2022;14(628):eabi9196. doi:10.1126/scitranslmed.abi9196

130. Ganassi M, Zammit PS. Involvement of muscle satellite cell dysfunction in neuromuscular disorders: Expanding the portfolio of satellite cell-opathies. *Eur J Transl Myol*. Mar 18 2022;32(1)doi:10.4081/ejtm.2022.10064

131. von Maltzahn J, Jones AE, Parks RJ, Rudnicki MA. Pax7 is critical for the normal function of satellite cells in adult skeletal muscle. *Proc Natl Acad Sci U S A*. Oct 8 2013;110(41):16474-9. doi:10.1073/pnas.1307680110

132. Bankole LC, Feasson L, Ponsot E, Kadi F. Fibre type-specific satellite cell content in two models of muscle disease. *Histopathology*. Dec 2013;63(6):826-32. doi:10.1111/his.12231

133. Wanschitz JV, Dubourg O, Lacene E, et al. Expression of myogenic regulatory factors and myo-endothelial remodeling in sporadic inclusion body myositis. *Neuromuscul Disord*. Jan 2013;23(1):75-83. doi:10.1016/j.nmd.2012.09.003

134. Jensen KY, Nielsen JL, Schroder HD, et al. Lack of muscle stem cell proliferation and myocellular hypertrophy in sIBM patients following blood-flow restricted resistance training. *Neuromuscul Disord*. Jun 2022;32(6):493-502. doi:10.1016/j.nmd.2022.04.006

135. Hanna MG, Badrising UA, Benveniste O, et al. Safety and efficacy of intravenous bimagrumab in inclusion body myositis (RESILIENT): a randomised, double-blind, placebo-controlled phase 2b trial. *Lancet Neurol*. Sep 2019;18(9):834-844. doi:10.1016/S1474-4422(19)30200-5

Figure legends

Figure 1 Histological features and chemo- as well as cytokine expression in human inflammatory myopathies. (**A**) Trichrome staining showing endomysial inflammatory infiltrates (white arrowheads) as well as muscle fiber atrophy and endomysial fibrosis (black arrowheads), which is most severe in this case of IBM. Yellow arrowheads: rimmed vacuoles. Immunohistochemistry (brown signal): $CD3^+$ T cells occasionally invading intact muscle fibers in PM and IBM (blue arrowheads); $CD20^+$ B cells are most frequent in DM, but are occasionally also seen in PM and IBM; $CD68^+$ macrophages are frequent in all IIMs; phospho-TDP43-, p62- and ubiquitin-positive inclusions in IBM (black arrowheads). (**B**) Heatmap of chemo- and cytokine expression in PM, DM and IBM compared to controls. P-values were determined using the two-tailed Mann-Whitney test and are shown if the expression was significantly different from control after Bonferroni correction ($p<0.17$). Upregulation of LTα and LT-signaling target genes including *CCL19* and *CXCL10*. (**C**) Schematic drawing of LTα/LTβ heterotrimers and LTα homotrimers activation of both TNF and LTβ receptor, leading to the translocation of NF-κB into the nucleus. (**D**) In situ hybridization of LTα and LTβ receptor (LTβR). Controls (**i** and **ii**) show no LTα signal and little LTβR signal in muscle fibers (arrows in enlarged images shown *below* in **iii**). In IBM, little LTα is detected in inflammatory infiltrates (black arrowheads) as well as in myonuclei (black arrows in enlarged images shown *below* in **ii**). In IBM, LTβR is also detected in both, inflammatory infiltrates (black arrowheads) as well as in myonuclei (black arrows, in enlarged images shown below in **iv** as well as in another area in **v**). (**E**) Immunohistochemistry (brown signal) of LTβ in muscle cells of IBM cases (**ii-iv**) compared to controls (**i**). Bottom row shows zoomed-in areas of **i-iv**. LTβ is detected in inflammatory infiltrates (black arrowheads) in IBM. In muscle fibers, the overall LTβ signal is slightly increased in IBM with a particular enrichment in rimmed vacuoles (black arrows) and where lymphocytes infiltrate intact muscle fibers (white arrowheads). (**F**) Normalized read counts of *LTα, LTβ* as well as LT target genes *CXCL10, CXCL13, CCL5* and *CCL19* compared to the house keeping gene *HPRT1* in controls and IBM samples derived from two previously published RNAseq data sets, showing a strong and significant increase of LT-related gene expression.

Figure 2 Generation, histology and chemo-/cytokine expression of HSA-LTα/β transgenic mice. (**A**) Schematic drawing of the transgenic constructs of the coding sequences (CDS) of LTα and LTβ both being cloned downstream of the human skeletal muscle actin (HSA) promoter (-2000 to +239) followed by an SV40 poly A site. (**B**) Four founder mice carrying both transgenes, HSA-LTα and HSA-LTβ, and transmitting them through the germline were obtained (line #8, #19, #22, #44). (**C-D**) LTα and LTβ transgene expression was detected in quadriceps muscle fibers of HSA-LTα/β #19 mice by RNA *in situ* hybridization of paraffin sections (brown signal) in the muscle fibers at 3, 6 and 10 months of age and also in inflammatory infiltrates in skeletal muscle, shown at 10 months of age (**C**). LTα ELISA with skeletal muscle tissue homogenate from indicated time points and genotypes. Data are shown as ng LTα3/LTα1β2/LTα2β1 protein per mg total protein. Statistical significance was tested using two-tailed Student's t-test. (**E**) Histologically, HSA-LTα/β transgenic mice show endomysial inflammatory infiltrates and occasional muscle fiber necrosis. Especially at the age of 9 months, there is fibrosis and partial replacement by fatty tissue within the endomysium. Fiber size variation is also increased in transgenic mice (H&E and trichrome). In addition to the normal MHCI localization on endomysial capillaries seen in wild-type mice, transgenic mice display focal sarcolemmal MHCI upregulation (red signal). The inflammatory infiltrates are mostly composed of $B220^+$ B cells and $CD68^+$ macrophages and - to a lesser extent - of $CD4^+$ and $CD8^+$ T cells (brown signals). (**F**) Heatmap of chemo- and cytokine expression in HSA-LTα/β transgenic mice determined by quantitative PCR of quadriceps femoris muscle tissue at 3, 6 and 10 months of age. P-values were determined using two-tailed Mann-Whitney tests. In case of significant differences between wild-type and transgenic mice, the p-values are displayed between the group of wild-type and transgenic line of the respective age group. (**G**) Quantitative PCR determining LTα and LTβ expression in different organs of HSA-LTα/β transgenic mice. *P*-values were determined using the ANOVA test with Šídák's multiple comparison test, significant differences compared to wild-type are displayed. (**H**) HE-stained sections of three different muscles from 9 months old HSA-LTα/β mice.

Figure 3 Muscle fiber size distribution, muscle hypothrophy and motor impairment in HSA-LTα/β transgenic mice. (**A**) Muscle fiber diameters were examined morphometrically using cross sections of the quadriceps femoris muscle (at 3 months, 596 fibers of n = 4 wild-type (wt) and 840

fibers of n = 4 HSA-LTα/β transgenic mice (LT); at 6 months: 981 fibers of n = 4 wt mice and 1075 fibers of n = 5 LT mice; at 10 months: 1266 fibers of n = 5 wt mice and 1732 fibers of n = 5 LT mice). For statistical analysis, we used Chi-Square test and grouped fibers into atrophic (<50 µm), normal (50-109 µm) and hypertrophic (>109 µm). Fiber size distribution was broader in HSA-LTα/β transgenic mice at 3 and 6 months, with both, more atrophic and hypertrophic fibers; there were more atrophic fibers at 10 months of age. (**B**) Body weight was determined every 4 weeks and is displayed separately for female and male mice. (**C**) Weight of quadriceps femoris, gastrocnemius, and triceps brachii muscles. Two-sided unpaired Student's t-test was used for statistical analysis. Differences were significant for all analyzed time points for all muscles; **** = $p<0.0001$. Motor performance of wild-type and HSA-LTα/β transgenic mice was determined by the grip strength test (**D**) and by the hanging wire test (**E**). Groups were compared using the two-sided unpaired Student's t-test. *P*-values are shown in case of a significant difference.

Figure 4 Organelle stress and signs of altered autophagolysosomal pathways in chronic myositis. (**A-C**) Gene expression in HSA-LTα/β transgenic mice determined by quantitative PCR of quadriceps femoris muscle tissue at 3, 6 and 10 months of age. Expression of genes related to ER stress, autophagolysosomal pathway, heat shock response (**A**) as well as oxidative stress related genes (**B**) are displayed in heat maps. P-values were determined using two-tailed Mann-Whitney tests. In case of significant differences between wild-type and transgenic mice, the p-values are displayed between the group of wild-type and transgenic line of the respective age group. To better visualize the gene expression changes of the marked upregulated autophagy related gene *ATG5* at 6 months of age, we also displayed it together with another autophagy related gene *BECN1* and lysosomal protease *CTSB* in transgenic compared to wild-type mice in (**C**). Both autophagy related genes are upregulated at 3 months (*ATG5*) and 6 months (*ATG5, BECN1*, see (**A**), but downregulated (*ATG5*) along with lysosomal *CTSB* at 10 months. (**D**) Downregulation of *ATG5, BECN1* and *HSPB1* as well as upregulation of *CTSB* in human IBM muscle tissue compared to controls determined by analysing published RNAseq data. (**E-F**) We determined amounts of LC3-I and LC3-II proteins in muscle of 6 and 10 months old HSA-LTα/β transgenic compared to wild-type mice by Western blot (**E**) and observed a significant reduction of total LC3 and LC3-II/ α-tubulin ratio in transgenic mice at 6 months and a significant increase in total LC3 and a decrease

in the LC3II/ LC3-I ratio at 10 months. Quantification of Western blot bands (**F**); values for total LC3 and LC3II are relative to wild-type values; n=5 biological replicates at 10 months; 1-2 technical replicates from 3-4 biological replicates at 6 months. P-Values were determined using two-tailed student's t-tests. Dotted lines shows, where membranes were cut, solid line shows cropping for representation in this figure; full size membranes are shown in the supplementary figures. (**G**) In line with disturbed proteostasis, we occasionally observed focal accumulation of ubiquitin in muscle fibers of HSA-LTα/β transgenic mice at 6 and 10 months of age (immunohistochemistry). Distribution of LAMP2^{+} lysosomes was even in wild-type mice, but uneven with less, but larger lysosomes in HSA-LTα/β transgenic mice (immunohistochemistry). Scale bar = 50 µm. (**H**) Ultrastructural examination at 9 months of age did not show any IBM-like inclusions in HSA-LTα/β transgenic mice, but mitochondria showed slight swelling. Chi-Square test was used for statistical testing.

Figure 5 Behavioral and histological consequences of autophagy depletion in lymphotoxin-induced chronic myositis. (**A**) Breeding scheme to obtain HSA-LTα/β^{+} Ckmm-Cre^{+} Atg5$^{fl/fl}$ (HSA-LT;CreAtg5) mice. (**B-C**) Muscle volume was determined by magnetic resonance imaging (MRI) at 3 and 6 months of age of male and female HSA-LT;CreAtg5 compared to Ckmm-Cre^{+} Atg5$^{fl/fl}$ (CreAtg5) mice. Representative MRI (FLASH) images and 3D reconstructions of calf muscles are shown along with volumetric quantification. Muscle atrophy was observed in HSA-LT;CreAtg5 compared to CreAtg5 mice. Two-sided unpaired student's t-test was used to determine p-values. (**D-F**) Histological and immunohistochemical analysis for inflammatory markers revealed chronic myositis in HSA-LT;CreAtg5, but not in CreAtg5 mice, characterized by endomysial infiltrates composed of CD4^{+} and CD8^{+} T cells, B220^{+} B cells and CD68^{+} macrophages (brown signals) as previously observed in HSA-LTα/β transgenic mice. Sarcolemmal upregulation of MHCI were detected in HSA-LT;CreAtg5, but MHCI was either not (1 of 4) or expressed weakly/ only on single fibers (3 of 4) in CreAtg5 mice (red signal). Quantification is shown in F. P-values were determined using the ANOVA test with Šídák's multiple comparison test. (**G-H**) Motor performance of CreAtg5 and HSA-LT;CreAtg5 mice was determined by the grip strength test (**G**) and by the hanging wire test (**H**). Groups were compared using the two-sided unpaired student's t-test. P-values are shown.

Figure 6 Consequences of autophagy depletion in lymphotoxin-induced chronic myositis on proteostasis, ultrastructure and mitochondria. (**A**) Immunohistochemistry for ubiquitin, LAMP2, p62 and phospho-TDP43 (brown signals). HSA-LT;CreAtg5 mice show numerous ubiquitin- and p62-positive inclusions in all muscle fibers. Ubiquitin-positive inclusions were not observed in wild-type mice. One mouse showed little focal p62-positivity (n = 6 of 6 HSA-LT;CreAtg5 , but only focally in n = 1 of 6 wild-type; p=0.0152, Fisher's exact test). The distribution of $LAMP2^+$ lysosomes in HSA-LT;CreAtg5 compared to wild-type with less, but often larger lysosomes in most fibers and increased lysosomal density in other fibers. Occasionally, phospho-TDP43-positive inclusions are observed in individual fibers of HSA-LT;CreAtg5 mice (n = 6 of 6 HSA-LT;CreAtg5, Fisher's exact test when compared to wild-type: p=0.0152). (**B**) Electron microscopy at 6 months of age revealed disintegration of sarcomeric structure/ myofibrils (**i**), accumulation of granular and fibrillar material (between black arrows in **ii** and **iii**), probably corresponding to myofibrillar fragments, often containing inclusions resembling tubulofilamentous inclusions characteristic for human IBM (between black arrows in **iv**), diameter measured in d: 106 tubulofilaments showed a mean diameter of 16.9 +/- 2.3 nm in n=3 HSA-LT;CreAtg5 mice. Subsarcolemmal accumulation of mitochondria (**v**) next to accumulation of granular material (black arrowheads in **vii**) with foci of mitochondria in different stages of abnormal mitophagy (**vii**) with some mitochondria showing almost normal structure of cristae (black arrows in **vii**) and those with cristae remnants in double membranes characteristic for autophagosomes (abnormal mitophagy, white arrowheads in **vii**). Focal deposits of abnormal myelin-like phospholipid are frequently seen (**viii**). Pyknotic, abnormally invaginated myonucleus (**ix**). Scale bars are 500 nm. (**C**) Long-read nanopore sequencing of PCR amplified mitochondrial DNA, showing no obvious deletions in any of the genotypes tested. Coverage is displayed in gray. Single nucleotide substitutions are shown in green (adenine), orange (guanine), blue (cytosine) and red (thymine). (**D**) Combined cytochrome c oxidase (COX, brown signal) succinate dehydrogenase (SDH, blue signal) enzyme histochemistry. Even distribution of COX-positive mitochondria in wild-type (**i**) with higher density in type 1 fibers (brown signal). Focal irregularities in the distribution of COX-positive mitochondria in HSA-LTα/β (**ii**), more pronounced in HSA-LT;CreAtg5 mice that also display single fibers with mosaic COX-positive (brown) and COX-negative mitochondria (blue, due to preserved SDH activity, black arrowheads,

iii and **iv**, with zoom-in of these fibers to the right of **iii** and **iv**. Several fibers also focally lack both, COX and SDH activity (black arrows).

Figure 7 Transcriptional consequences of depleting autophagy in lymphotoxin-induced chronic myositis mice. (**A-D**) Heatmaps of gene expression in wild-type, CreAtg5, HSA-LTα/β and HSA-LT;CreAtg5 mice determined by quantitative PCR of quadriceps femoris muscle tissue at 6 months of age. P-values were determined using Mann-Whitney-U test and are displayed above the group of mice in case of a significant difference after Bonferroni correction (*p*-values <0.016). Cyto- and Chemokine expression is shown in A, ER stress and autophagolysosomal gene expression is displayed in (**B**). (**C**) Genes related to muscle de- and regeneration and Alzheimer disease/ neurodegeneration including *App* and *Cryab*. (**D**) Genes related to oxidative stress. [Gene functions overlap.]

Figure 8 IBM-like myositis in mice is resistant to anti-inflammatory treatments. (**A**) Timeline of treatment. Density of $CD3^+$ T cells in the liver of untreated mice and after treatment; for anti-Thy1.2 (**B**) and prednisolone (**C**) treatment. P-values were determined using two-tailed Students t-tests. Grip strength of mice at day 150. The results show genotype-dependent differences, but no treatment effect after prednisolone (**D**) and anti-Thy1.2 (**E**) treatment. (**F**) The heatmap shows expression examined by qPCR relative to the respective untreated controls (treated compared to untreated wild-type, HSA-LTα/β and HSA-LT;CreAtg5, respectively) – here in case of prednisolone treatment. Except for a significant downregulation of *Cxcl10, Ncf2* and *Gpx2* following prednisolone treatment of HSA-LTα/β mice compared to untreated HSA-LTα/β and non-significant trends for some other genes, there was a counterintuitive upregulation of *Ccl5* in treated compared to untreated HSA-LT;CreAtg5 mice, but otherwise stable gene expression. *n.d.* = not determined. Mann-Whitney-U test was performed as statistical test since some values were not normally distributed. P-values are only displayed in case of statistical significance between untreated and treated mice. Behavioral phenotypes and gene expression patterns following these treatments were stable (see also Supplementary figures).

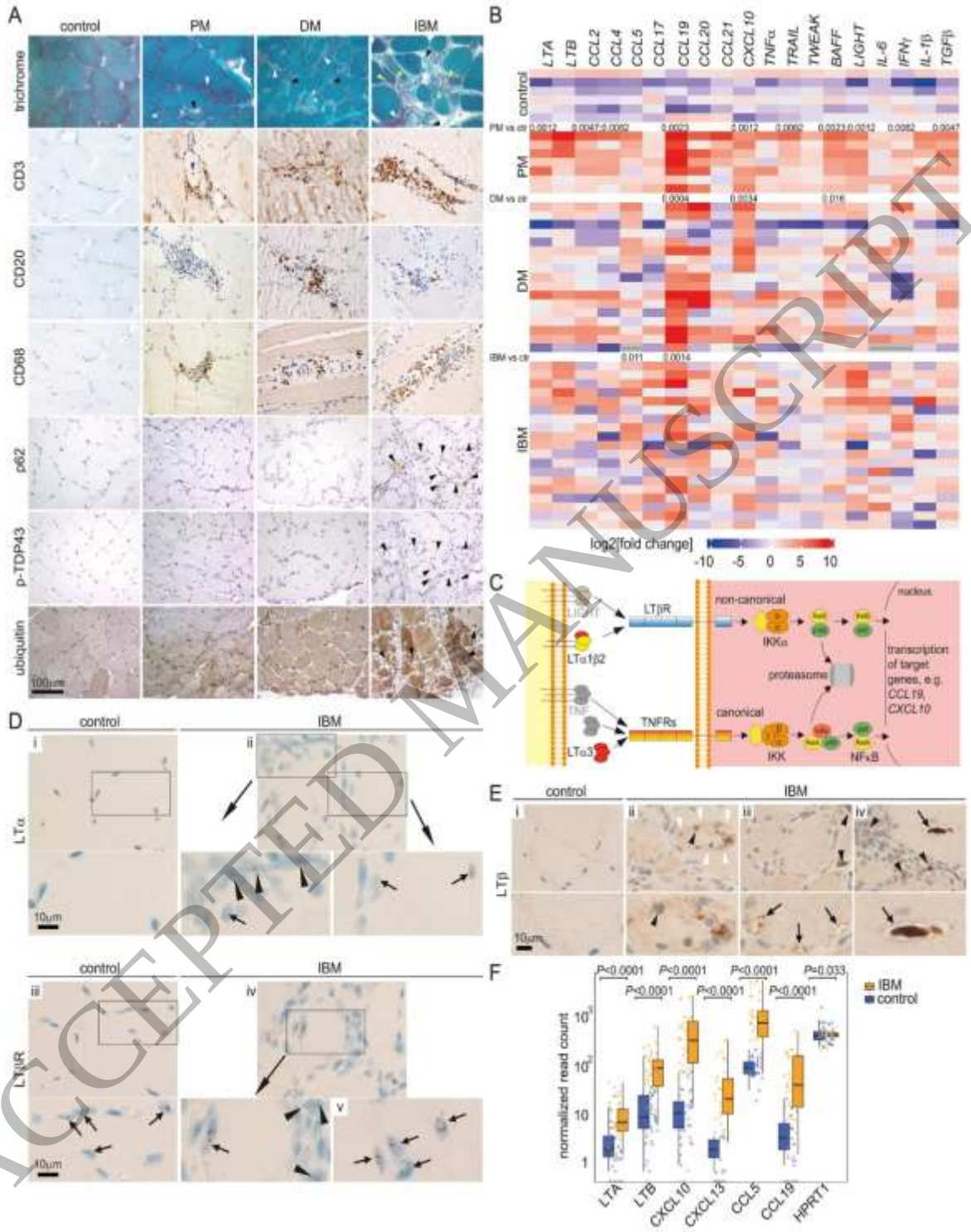

Figure 1
185x213 mm (x DPI)

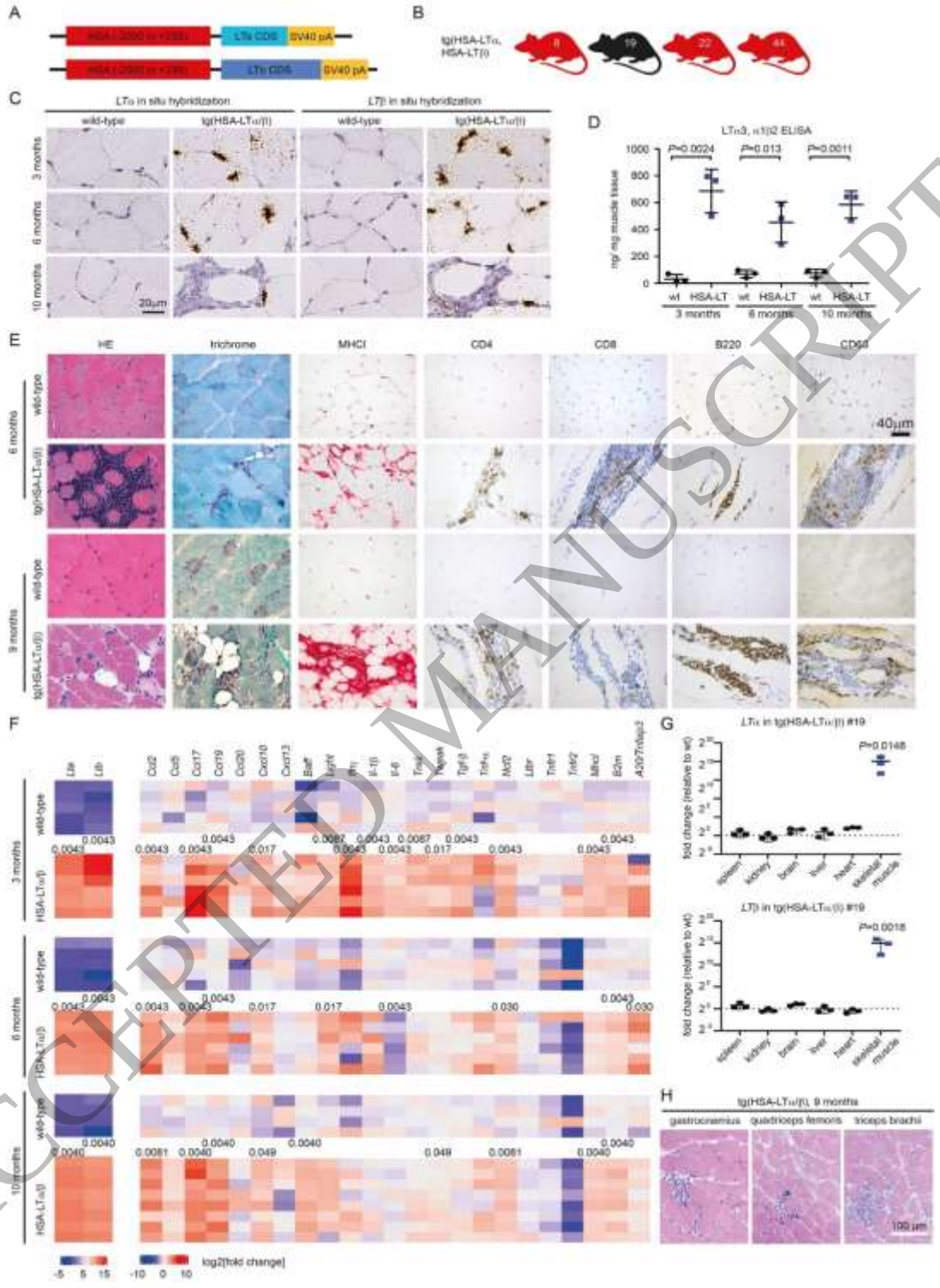

Figure 2
185x266 mm (x DPI)

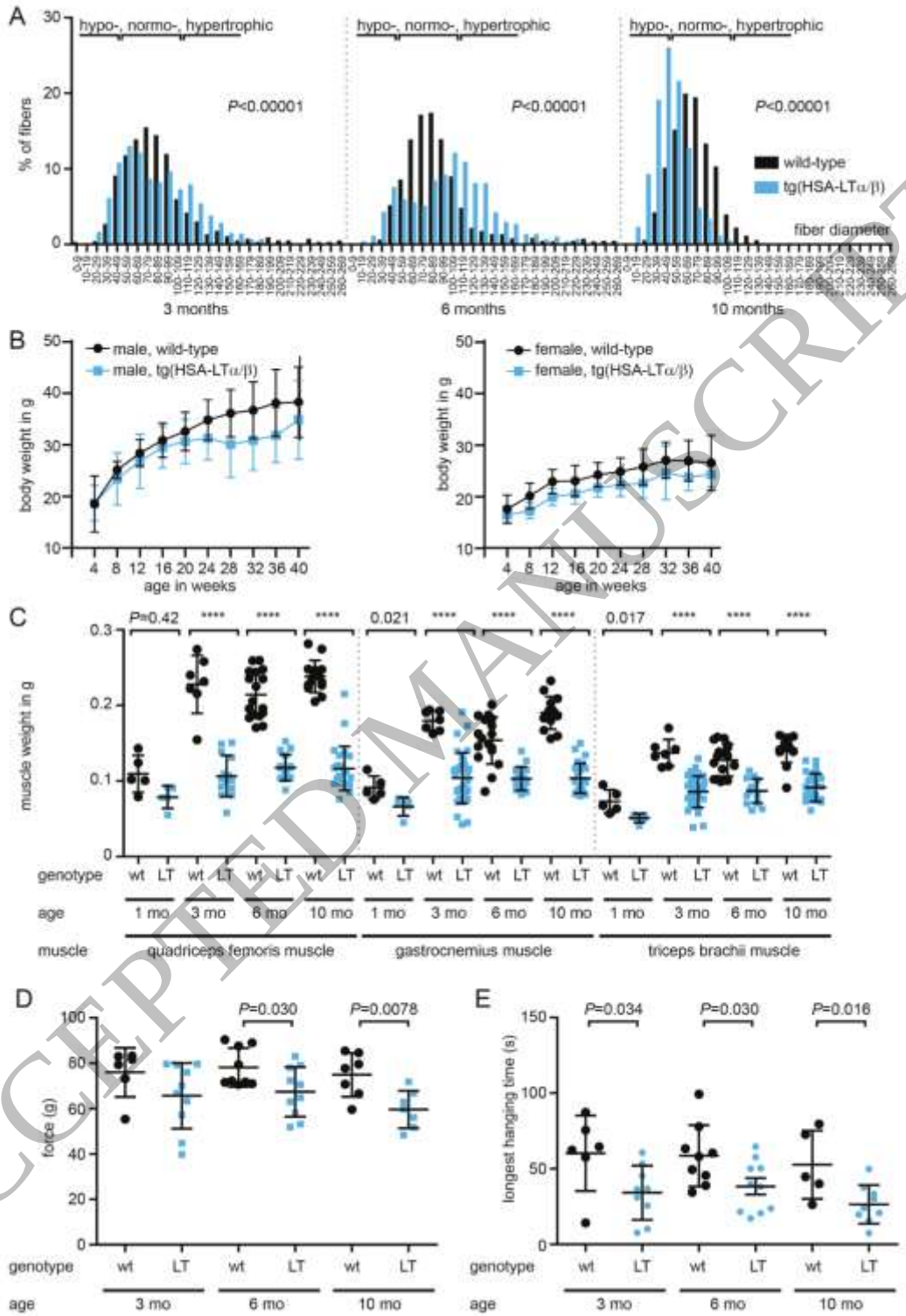

Figure 3
185x267 mm (x DPI)

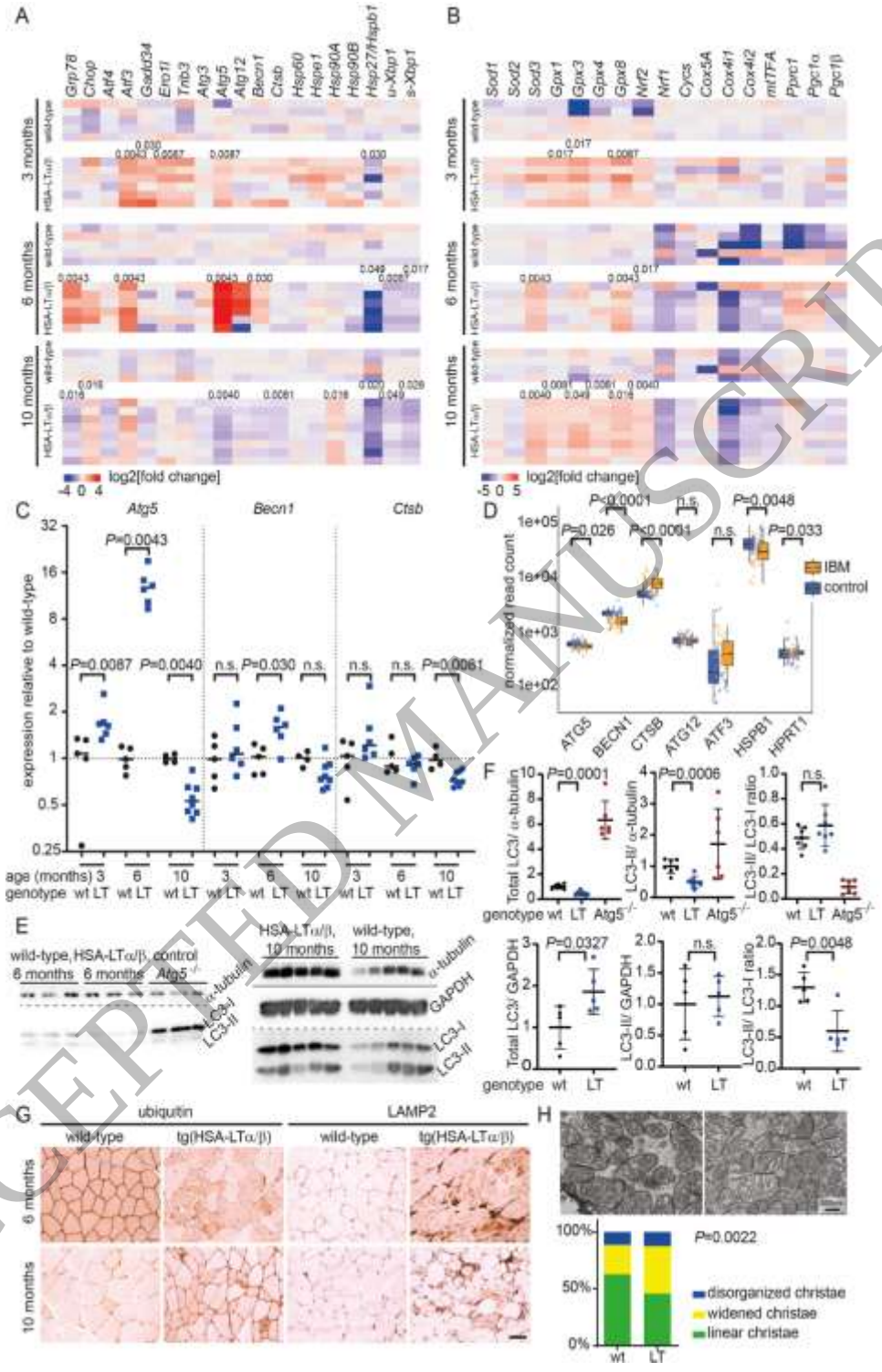

Figure 4
185x272 mm (x DPI)

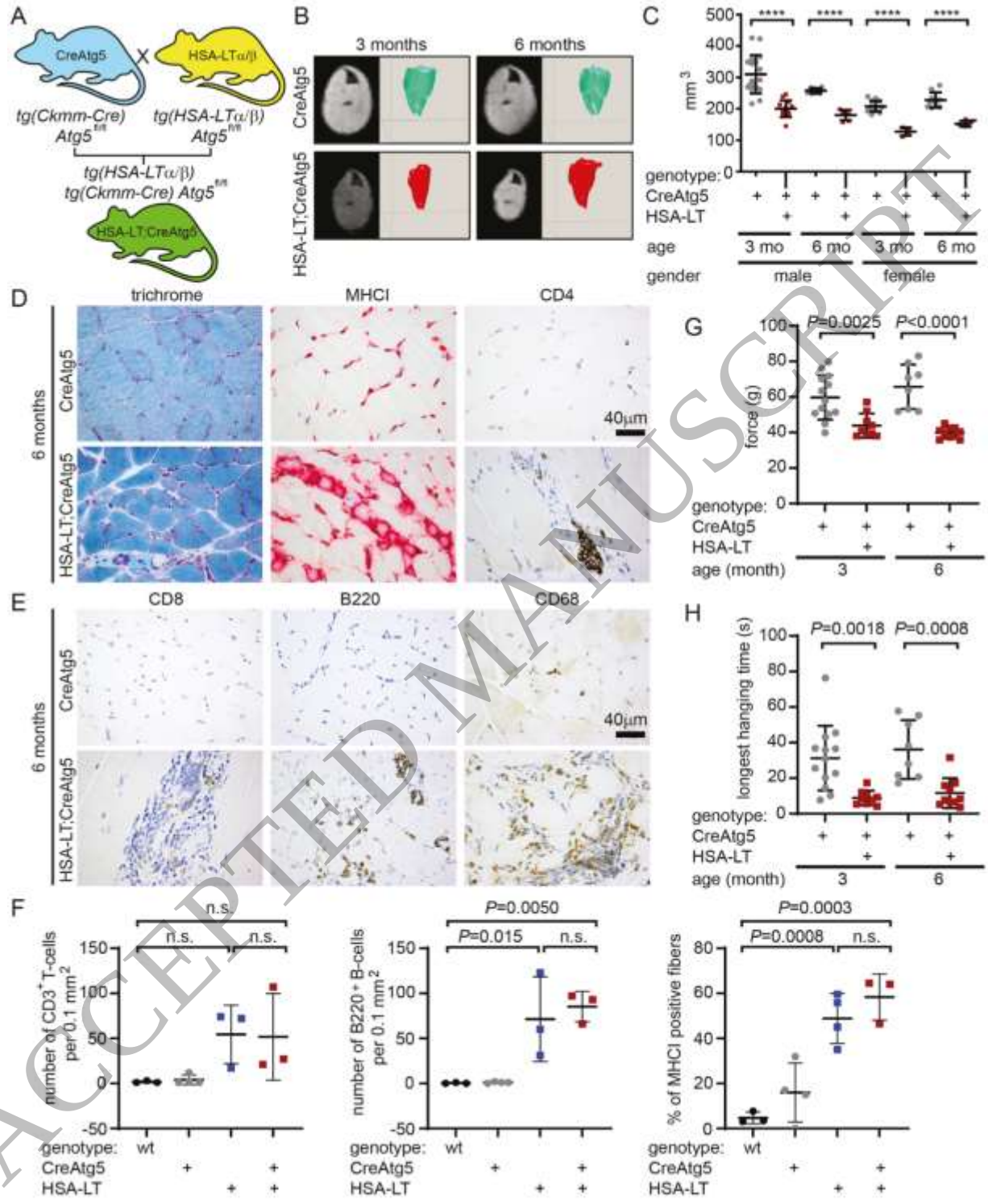

Figure 5
185x233 mm (x DPI)

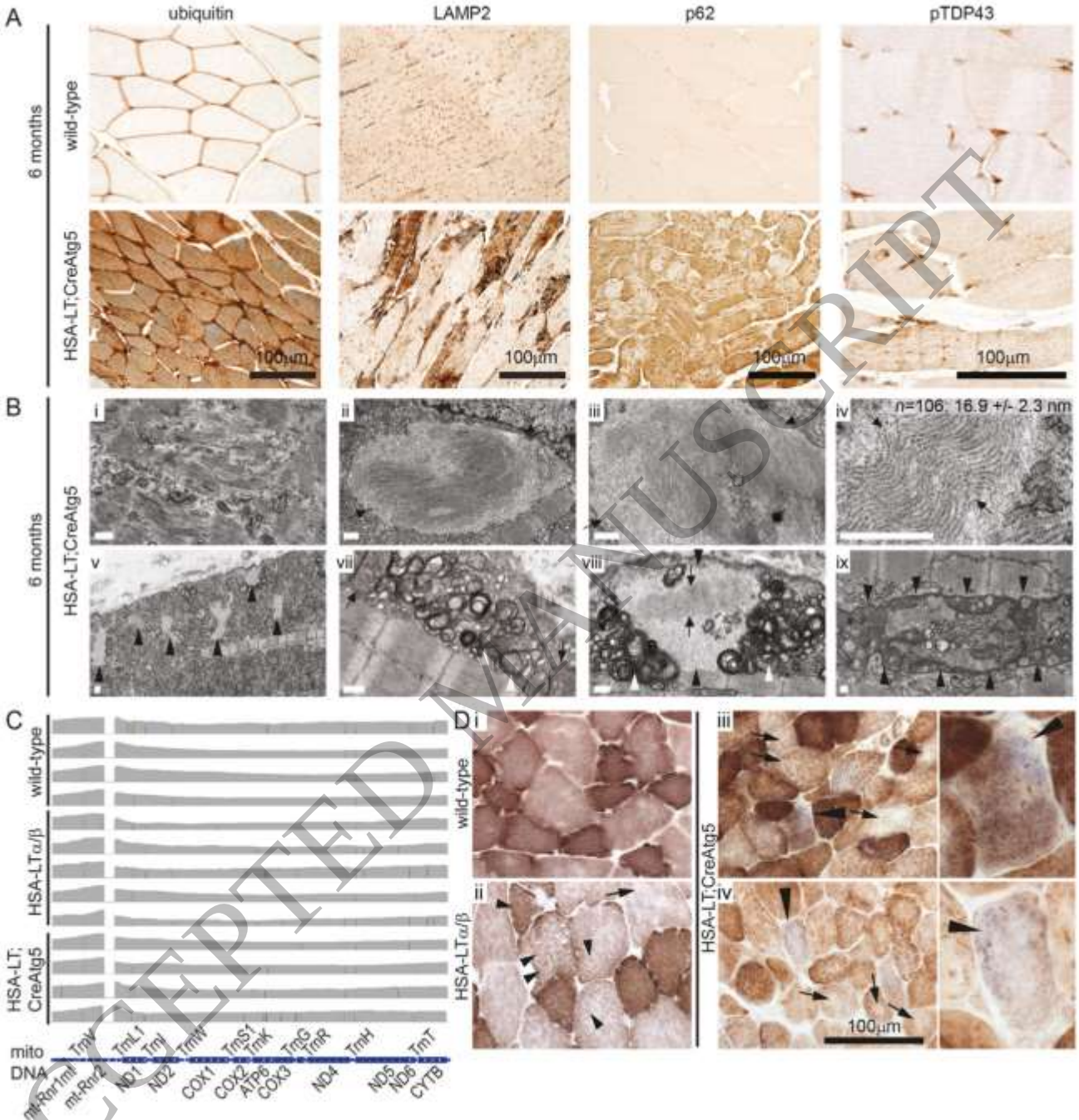

Figure 6
185x189 mm (x DPI)

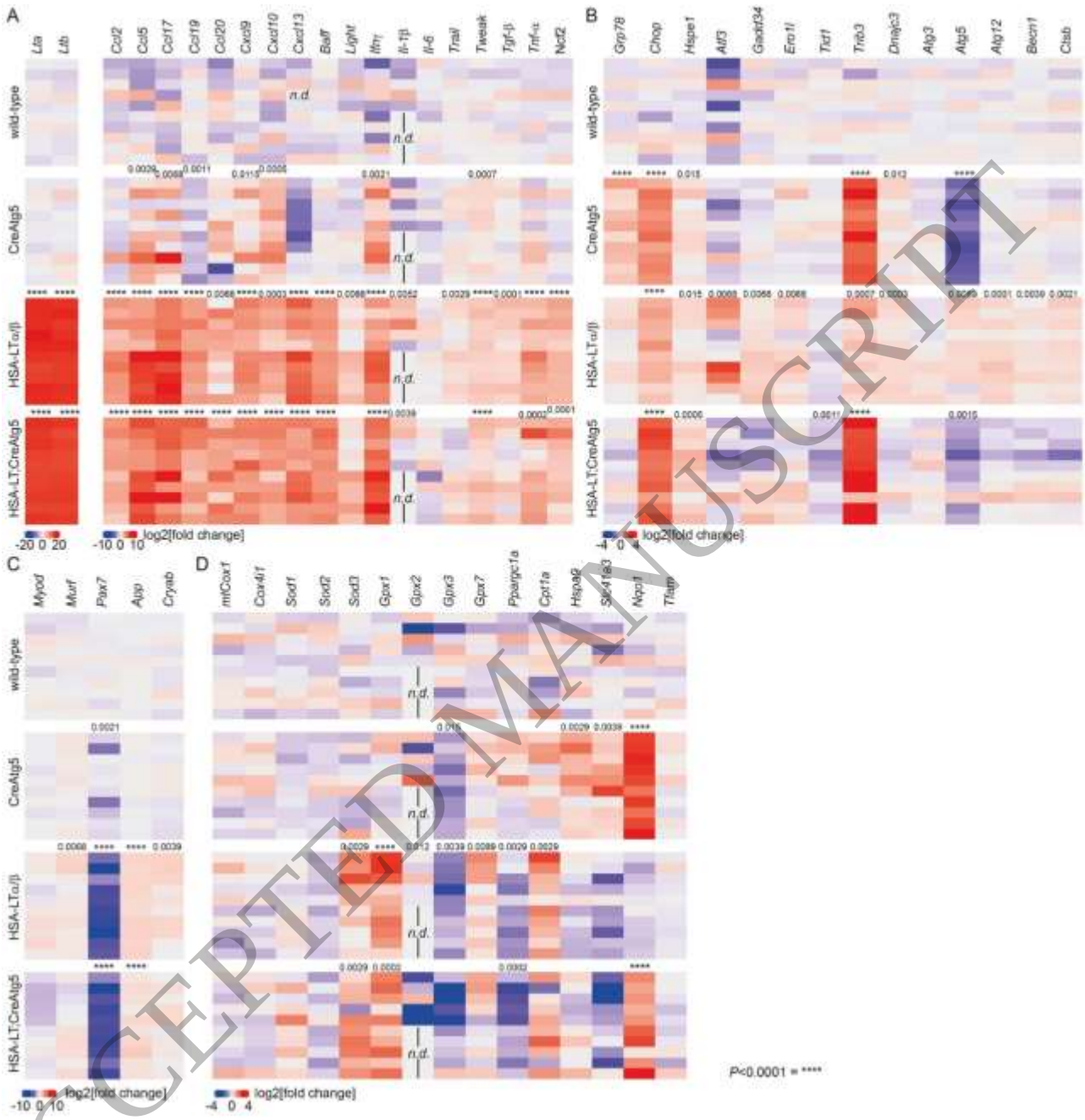

Figure 7
185x188 mm (x DPI)

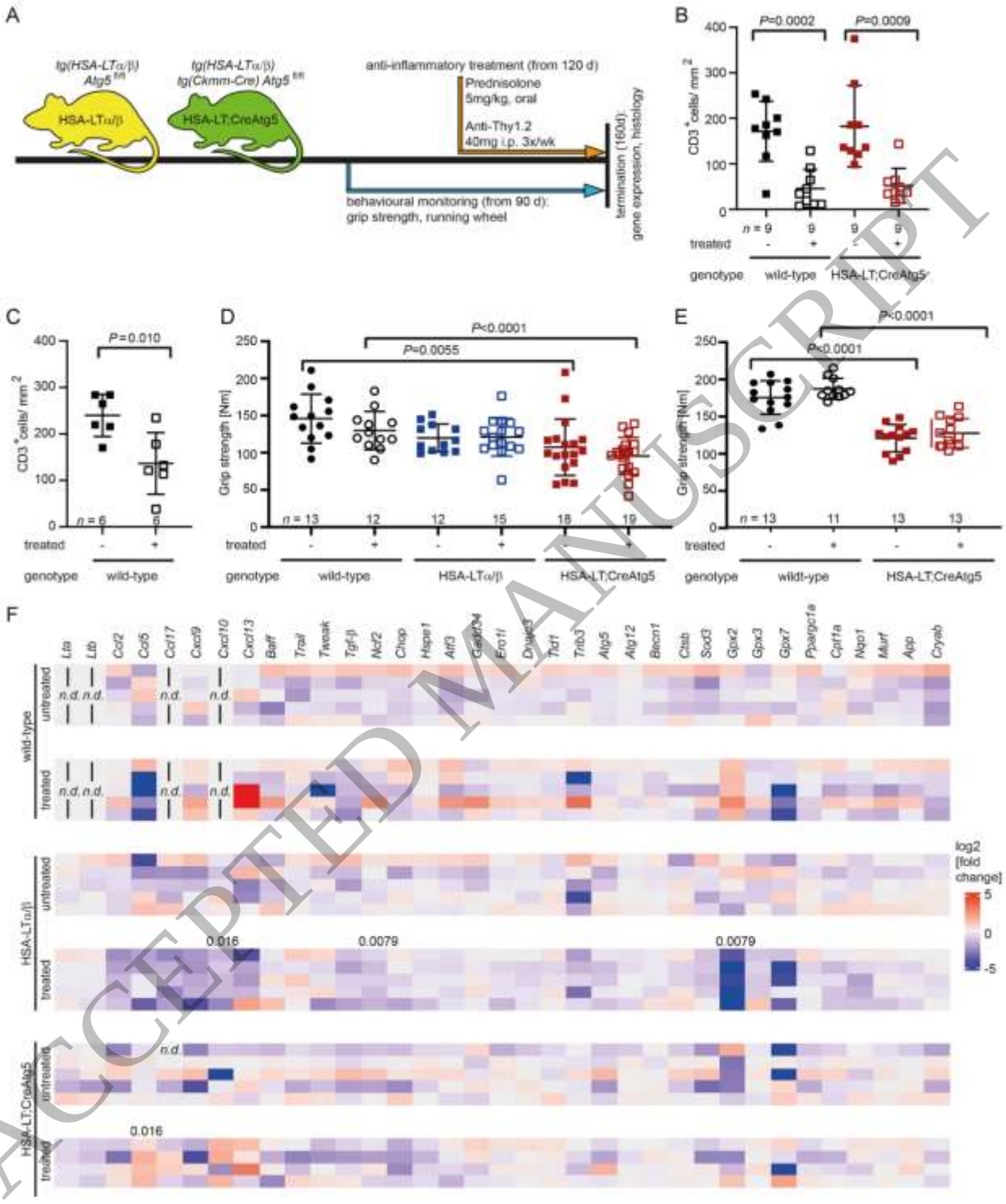

Figure 8
185x221 mm (x DPI)